京都大学学術情報リポジトリ
KURENAI 紅
Kyoto University Research Information Repository

京都大学
KYOTO UNIVERSITY

| | |
|---|---|
| Title | Study on Compatibility of Advanced Materials Exposed to Liquid Pb-Li for High Temperature Blanket System( Dissertation_全文 ) |
| Author(s) | Park, Changho |
| Citation | Kyoto University (京都大学) |
| Issue Date | 2013-09-24 |
| URL | http://dx.doi.org/10.14989/doctor.k17916 |
| Right | 許諾条件により要旨・本文は2013-12-31に公開 |
| Type | Thesis or Dissertation |
| Textversion | ETD |

Kyoto University

# Study on Compatibility of Advanced Materials Exposed to Liquid Pb–Li for High Temperature Blanket System

CHANGHO PARK

# List of Contents

# List of Tables

# List of Figures

# 1. Introduction

## 1.1. Background

The International Energy Outlook 2011 (IEO2011) was presented an assessment by the U.S. Energy Information Administration (EIA) of the outlook for international energy markets through 2035 [1-4]. In the IEO2011 reports, the world-wide energy consumption will continue to increase by 2% per year. Figure 1.1(a) shows the actual values for energy consumption starting from 1990 until today and the predictions of the energy consumption until the year 2035. This means the world-wide energy consumption is predicted to be twice as high in the year 2035 compared to today (2011). However, world energy consumption by fuel (1990-2035) shows in Figure 1.1(b). With respect to global warming and energy depletion, each country has to make efforts to reduce the consumption of fossil fuels. The dramatic increase in world-wide demand for energy and its environmental problems are expected in nowadays and the future have stimulated international cooperation to consider how to meet future energy needs while reserving and improving the environment. This has led to nuclear energy, because large amounts of energy can be produced with nuclear reactors without the anti- environmental effects accompanied by the use of fossil fuel products. Although renewable energy sources (solar photovoltaic, biomass, wind power etc.) may offer similar beneficial effects, concerns exist on economic efficiency and reliability when they are used for base-load power generation. The technology and economic reliability of nuclear energy have been demonstrated by the practical reactor operation throughout the world today.

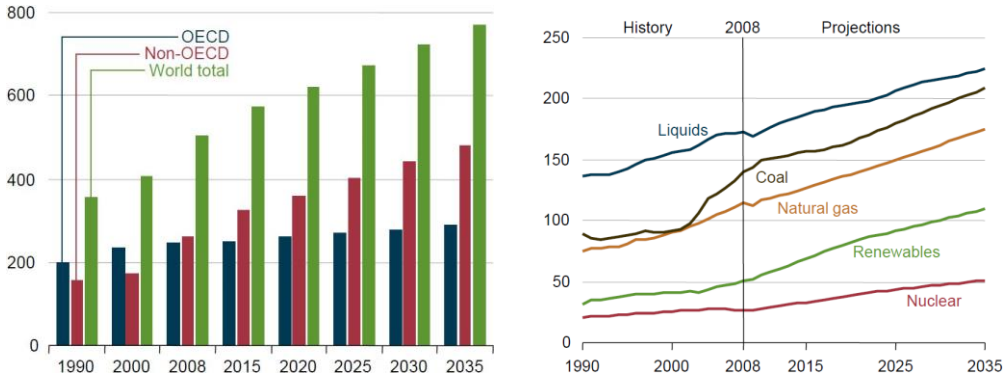


Figure 1.1 World energy consumption (a) and world energy consumption by fuel 1990-2035 (b) (quadrillion Btu, British thermal units) [1].

Currently, nuclear energy produces approximately 14% of the world's electricity supplies and approximately 6% of total energy used worldwide. The amount of total energy produced and of energy use per capita is increasing. The total energy requirements of the world increased by a factor of 2.5 between 1970 and 2006, from 6181 to 15311 GWa (195 to 483 exajoules (EJ)). Over the past decades, the share of electricity as a percentage of the total energy produced has also increased. Figure 1.3 shows the contribution of different energy sources to the global energy balance over this period. The share of nuclear grew from just below 0.5% in 1970 to above 7% in the 1990s and declined to 6% by 2006. Fossil fuels remain the dominant energy source [5].

Nuclear power has been used to produce electricity for public distribution since 1954. Since that time, power plants have been operated in 32 countries Currently, 30 countries operate 439 plants, with a total capacity of 372 GW(e). Further, 34 units, total 28 GW(e), are under construction (as of 26 June 2008). During 2007, nuclear power produced 2608 billion kW·h of electricity. The industry now has more than 13000 reactor years of experience. In Western Europe, nuclear generated electricity accounts for almost 30% of total electricity. In North America and Eastern Europe, it is approximately 18%, whereas in Africa and Latin America it is 1.8% and 2.6%, respectively. In the Far East, nuclear energy accounts for 11.5% of electricity generation; in the Middle East and South Asia it accounts for 1.6%. Nuclear energy use is concentrated in technologically advanced countries.

Nuclear energy has contributed to the economic developments as well as our convenient lives on the basis of stable electricity supply. About 30% and 15% of total electric power consumed in Japan and in the world, respectively, is now generated at nuclear plants, and its proportion is predicted to increase especially in developing countries like China and India. Nuclear energy is a promising option from the aspects of energy security as well as low $CO_2$ emission. The energy system depending on fossil fuels is vulnerable to future soaring prices of oil and natural gas and responsible to the global warming. Nuclear plants recently respond to some accessory demands of desalination of water or hydrogen production by utilizing the nuclear heat. After Fukushima accident in March this year, a radical overhaul of the energy policy in Japan including nuclear has been launched. Whatever a future direction of the policy given for nuclear energy is, efforts to resolve intrinsic technological challenges in the utilization of nuclear power are continuously necessary to advance the safety, the nonproliferation, and the management of spent fuels.

Advanced nuclear systems, such as fast breeder reactor and fusion reactor, have been developed to increase the thermal efficiency. For the development of advanced nuclear systems, an essential issue is the performance of the structural materials. Key technologies for the structural materials include high temperature strength and long life time with the resistance under high corrosive and neutron dose environment. Many advanced materials with high performances, such as reduced activation ferritic/martensitic (RAFM) steel, vanadium alloy, SiC/SiC composite, have been researched and developed as structural materials, blanket for fusion. Structural materials, RAFM steels are considered to the final candidate of the international thermo-nuclear reactor (ITER) that blanket module and materials R&D to evaluate the performance under irradiation have been conducted as an international collaboration research of the broader approach (BA). In this activity, it was shown that the most critical issue for RAFM steel fabrication of ITER-TBM is welding and joining technology because the total fusion lines of welding is estimated to the 500 m per a body of fusion blanket of DEMO reactor.

## 1.2. The necessity of nuclear energy

### 1.2.1. Fusion reactor system

Fusion is an attractive option for future large-scale energy production due to the abundant quantities of the basic fuels - deuterium and lithium - as well as to its inherent safety features and to waste production that will not be a long-term burden for future generations. Moreover, fusion offers the possibility of an environmentally friendly energy supply due to the absence of greenhouse gas emissions. In the sun and other stars, huge gravitational forces compress the nuclei of hydrogen atoms close together to overcome their mutual electrical repulsion. The nuclei then fuse, releasing the energy that lights and warms the universe. A gas consisting of a mixture of hydrogen isotopes (deuterium and tritium) is heated to a temperature high enough to strip the electrons from the atoms. The resulting medium consists entirely of charged particles. This is called "plasma". The plasma is electrically conducting and therefore can be confined by strong magnetic fields. When heated to temperatures around 100 million degrees, energetic collisions between the plasma ions produce fusion reactions.

Among the fusion reactions, the following reaction (Eq. 1.1) has been considered to be most adequate for near-future realization of fusion energy. This fusion reaction occurs

between the nuclei of the two heavy isotropes of hydrogen – deuterium (D) and tritium (T) – to form a helium nucleus and the release of a neutron and high energy;

$$^{2}D_{1} + {}^{3}T_{1} \rightarrow {}^{4}He_{2}\,(3.5MeV) + {}^{1}n_{0}\,(14.1MeV) \qquad (1.1)$$

The magnetic storage configuration is needed to control the thermo-nuclear plasma sustained by this reaction. Although many fusion reactor concepts have been developed, the most typical one will probably be Tokamak type [6]. For its advance and development, international cooperation was established to organize the international thermo-nuclear reactor (ITER) taken by China, the European Union, India, Japan, Korea, Russia and the United States.

ITER project was focused on plasma science and technology and the mission did not include a complete set up of blankets for energy generation. A part of blankets will be assembled as a test blanket module (TBM). In BA program, as mentioned in section 1.1, compatibility at environment were acknowledged as a prime problem of satisfy for TBM. In future reactors, two components are particularly important; the tritium-breeding blankets (TBB) and divertor. The TBB takes a role in extraction the fusion energy. And it has to produce tritium for a self-sufficient operation. The divertor purifies the plasma by locally creating a magnetic configuration to evacuate the α-particles and impurities and also extracts fusion energy. A summary of structural materials for fusion blanket and divertor is given in Table 1.1 [7].

Table 1.1 Main candidate materials for plasma facing and breeding blanket components [7].

| Function | First wall | Breeding blanket | Divertor |
|---|---|---|---|
| Plasma facing material | W-base alloy,<br>W-coated ODS steel,<br>flowing liquid metal: Li | - | W-base alloy, W-coated SiC/SiC<br>flowing liquid metal: Li, Ga, Sn, Sn–Li, eutectic Pb–Li |
| Neutron multiplier material | - | Be, $Be_{12}Ti$, $Be_{12}V$, Pb | - |
| Tritium breeding material | - | Li, eutectic Pb–Li,<br>Li-base ceramic material ($Li_2O$, $Li_4SiO_4$, $Li_4SiO_4$, +2.5 wt.%$SiO_2$, $Li_2TiO_3$, $Li_2ZrO_3$, $LiAlO_2$) | - |
| Structural & functional material | RAFM steel, ODS steel, Vanadium alloy, SiC/SiC | RAFM steel, ODS steel, Vanadium alloy, SiC/SiC | ODS steel, W-base alloy, SiC/SiC |
| Coolant | - | Water, helium,<br>eutectic Pb–Li, Li | Water, helium, eutectic Pb–Li |

## 1.3. Components of nuclear fusion reactor

### 1.3.1. Blanket system

The blanket is the component which will be located between the fusion plasma and vacuum vessel and provides the main thermal and nuclear shielding to the vessel and other components. This component may correspond to the reactor core of the fission plant where neutron energy is converted into the heat which is removed by coolants. The blanket also works as tritium producer and thermal generator in the fusion reactor. To realize these goals, many different concepts were proposed. All of the DEMO concepts could be classified with regard to the breeding materials into two categories [8-12]: solid ceramic and liquid breeders with the options of self-cooled or separately cooled versions. These concepts also depend on development of structure materials and the design parameters, such as thermal exchange ratio, neutron flux and Tritium Breeding Ratio (TBR). The main functions of blanket are:

1) The generation and transport of heat

2) The tritium breeding (recycle of tritium)

3) The neutron shielding

Major fraction of fusion energy is transported by neutrons which energy is converted to the heat by reactions with the structural material and coolant of the blanket. Thus, the design of the blanket is a quite complex task because thermal, structural, and neutronics analyses are required. In addition, because of serious damages given by the fast neutron radiation, a periodic replacement is unavoidable. Hence, the maintenance scheme should be in consideration for the components design [13]. Aspects of present blanket designs are summarized in Table 1.2. A good reference for the review of many blanket designs and technologies can be seen in [14]. Examples of major blanket designs are summarized in the following sections.

Table 1.2 Summary of present blanket designs.

| Name | Water cooled solid breeder [15] | Flibe [16] | HCLL [13] | DCLL [17] | HCPB [13] |
|---|---|---|---|---|---|
| Coolants | Water | Flibe | He | He, Pb–Li | He |
| Breeding materials | $Li_4SiO_4/Li_4SiO_4$ | Flibe | Pb–Li | Pb–Li | $Li_4SiO_4/Li_2TiO_3$ |
| Neutron multiplier | $Be/Be_{12}Ti$ | Flibe | Pb–Li | Pb–Li | Be |
| Radiation shield | Water | $B_4C$ | Pb–Li | Pb–Li | - |

| | | | | | |
|---|---|---|---|---|---|
| Outlet temperature | 325℃ | 550℃ | 500℃ | 500℃ | 500℃ |
| Structure | F82H | JLF-1 (Fe–9Cr–2W) | EUROFER (9%CrWVTa) | RAFM | EUROFER (9%CrWVTa) |

#### 1.3.1.1. Solid breeder and water cooled design

Water is commonly used as the coolant for many applications because of its low cost and well-known physical properties. Slim-CS, the DEMO design by JAERI, employs water cooling for the blanket and divertor. Technical concerns of the water cooling are its low energy conversion efficiency (~30%) and tritium absorption as HTO. In addition, the presence of water in the blanket decreases the tritium breeding ratio, thus large amounts of neutron multipliers such as beryllium is required as shown in Figure 1.2.

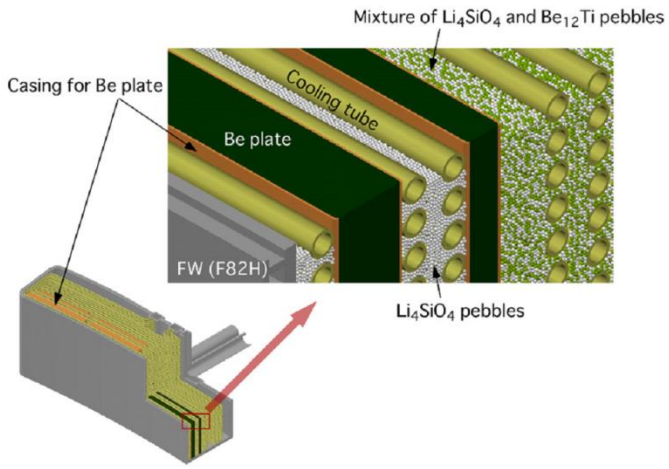


Figure 1.2 Slim-CS blanket contains Be plate and $Be_{12}Ti$ pebbles for the neutron multiplication [18].

#### 1.3.1.2. Flibe blanket design

Flibe is a molten salt material where both Li (breeder) and Be (multiplier) are connected with Fluorine for example as $(LiF)_2(BeF_2)$. Flibe shows low electrical conductivity which is preferred for small MHD pressure drop; however its low thermal conductivity about 1 W/m/K at 500ºC is not preferred. Although Flibe has a small chemical reactivity with air and water compared with other candidates, its high melting point of 459℃ and low tritium inventory make the use of this material challenging.

#### 1.3.1.3. Lithium–lead breeder and coolant design

Lithium–lead (Pb–Li) works as breeder, coolant, neutron multiplier and shield. Despite of its demerit the of strong MHD pressure drop, many advantages make it attractive to researchers. Pb-Li has good heat transfer properties, high temperature capability for high energy conversion efficiencies, low chemical reactivity and smooth tritium extraction property. In addition, its low pressure (~2 MPa) eases the requirement to the structure design. Two designs using Pb–Li coolant from references are introduced in the following sections.

(1) He cooled lead lithium blanket (HCLL) [13]

One disadvantage of liquid metal coolant is the pressure drop caused by the MHD force. When the coolant flows perpendicular to the magnetic field, electric current is generated by the electromagnetic induction. These relations follows Fleming's right hand rule. Then generated current and the existing magnetic field cause the Lorentz force to the coolant to the direction against the flow. This force causes the MHD pressure drop, which results large pumping power or unallowable condition to flow. Several means are known to ease this effect. Surrounding coolants by insulator is one of these means and installed to the DCLL blanket design. HCLL design, in contrast, takes more conservative way to reduce the MHD pressure drop. Pb–Li in the blanket merely flows, so they don't work as coolant. Instead, pressurized helium in the structural steel works as coolant. This design is being proposed for the ITER TBM by EU nations.

(2) Dual coolant lead lithium blanket (DCLL) [17]

Dual coolant lead–lithium (DCLL) blanket is proposed by United States for the ITER-TBM and also DEMO. In order to reduce the strong MHD pressure drop of Pb–Li flow, a SiC flow channel insert (FCI) is assumed. Temperature of Pb–Li is maintained between 350–700ºC in order to keep its steel structure under 550℃.

Table 1.3 High temperature blanket designs and key parameters [19].

| | ARIES-AT | TAURO | A-SSTR-2 | A-HCPB | W/Li/He | EVOLVE | V/Li/He | V/Li | FFHR-2 | A-DC | ARIES-ST | FDS-II | FDS-III |
|---|---|---|---|---|---|---|---|---|---|---|---|---|---|
| Fusion power (GW) | 1.7 | 3 | 4 | 4.5 | 3.5 | 3.5 | 1.9 | 2.43 | 1 | 3.4 | 2.9 | 2.5 | 2.6 |
| FW heat flux ($MW/m^2$) | 0.26(ave) | 0.5(ave) | 1.0(ave) | 0.6(peak) | 2(peak) | 2(peak) | 0.3 | 0.1 | 0.1 | 0.45(ave) | 0.46(ave) | 0.54(ave) | 0.8(ave) |
| Neutron wall loading ($MW/m^2$) | 3.2(ave) | 2(ave) | 6(ave) | 2.76(ave) | 7(peak) | 10(peak) | 2.9(ave) | 2.5(ave) | 1.7 | 2.27(ave) | 4.1(ave) | 2.72(ave) | 4(ave) |
| Structure material | SiC/SiC composites | | | | W-alloy | | | V-alloy | | | RFAM | | |
| Maximum allowed temperature | 1000 | 1000 | 1100 | 1000 | 1400 | 1400 | 700 | 700 | 700 | 550 | 550 | 550 | 550 |
| FW material, Kth (W/mk) | 20 | 15 | 15 | 15 | 85 (at 1400K) | 85 (at 1400K) | 35 | 27 (at 700K) | 35 | 33 | 33 | 33 | 33 |
| Fuel form | L | L | S | S | L | L | L | L | L | L | L | L | L |
| Tritium breeder (neutron multiplier) | Pb–Li | Pb–Li | $Li_2TiO_2$(Be) | $Li_4SiO_4$(Be) | Li | Li | Li | Li | Flibe(Be) | Pb–Li | Pb–Li | Pb–Li | Pb–Li |
| Coolant | Pb–Li | Pb–Li | He | He | He | Li | He | Li | Flibe | He/Pb–Li | He/Pb–Li | He/Pb–Li | He/PbLi |
| Coolant $T_{in}$ | 654 | 650 | 600 | 350 | 800 | ~800 | 400 | 250 | 450 | 480 (Pb–Li) | 550 (Pb–Li) | 480 (Pb–Li) | 400 (Pb–Li) |
| Coolant $T_{out}$ | 1100 | 850 | 900 | 700 | 1100 | 1200 | 650 | 650 | 700 | 700 (Pb–Li) | 700 (Pb–Li) | 700 (Pb–Li) | 1000 (Pb–Li) |

Table 1.4 Advantage and disadvantage of structure material for high temperature blanket designs.

| | Advantage | Disadvantage |
|---|---|---|
| SiC/SiC composites | Good temperature properties | Required behavior and performance at high temperature and under irradiation, the fabrication and joining technology, etc. |
| V-alloy | Advantage of the excellent compatibility between V-alloy and lithium<br>Capability to accommodate high heat fluxes, low decay heat, low activation | Not suitable for the high temperature requirement due to relatively low outlet temperature |
| W-alloy | Avoids the compatibility issue between helium impurities and V-alloy | Due to the generation of 108m RE from nuclear interaction with base elements in the W-alloy, the goal of class-C waste disposal at the end of reactor life cannot be satisfied |
| RAFM | It is considered to be the primary structural material candidate for future fusion power reactors due to superior swelling resistance and excellent thermal and mechanical properties, but the upper engineering temperature limit is relatively low only about 550°C. | The higher exit temperature cannot be available because higher temperature can lead to higher thermal gradient and thermal stress across the FCIs, or lead to higher temperature of the structural material beyond the engineering limit for RAFM. |

The “multilayer flow channel inserts (MFCI)” with thermal insulating and electricity insulating and good chemical compatibility with Pb–Li are considered to be inserted in the coolant flow channels. Low temperature Pb–Li flows into the channel, then meanders through the multilayer flow channel inserts.

Table 1.5 Conclusions on attractiveness based on today's knowledge [14].

| | TSP | DAP | AAP | Comment |
|---|---|---|---|---|
| Ceramic breeder concepts (steel structures) | High | High | Medium–low | Little extrapolation of technology required, promising near term characteristics, potential for advanced power plants is limited unless significant progress with alternative multipliers and compatibilities is made |
| Ceramic breeder concepts (SiC/SiC structures) | Low | Very low | High | In principle a very advanced, attractive concept with good efficiency, but it remains to be seen if SiC-composites can be developed and qualified as structural material (FW!).<br>Hermeticity to high pressure Hemay not be achievable. Be and tritium control issues need to be addressed |
| Dual coolant concept (steel structures) | Medium (high for HCLL) | High | High | Good compromise between required development and performance, with potential for both, an attractive DEMO and advanced power plant |
| Self-cooled Pb–Li (SiC/SiC structures) | Low | Very low | Very high | In principle a very advanced, attractive concept with exceptional high efficiency, but it remains to be seen if SiC-composites can be developed and qualified as structural material (FW!) |
| Flibe | Medium | Medium | Medium–low | Performance limited (poor heat transfer characteristics), requires structural material allowing high operation temperature, difficult chemistry necessary to ensure compatibility with structural material |
| Helium | Very low | Very low | Very high | Exotic concept for very advanced power plants with neutron wall load > 6 $MW/m^2$, questionable if tungsten alloys can be qualified as structural material |

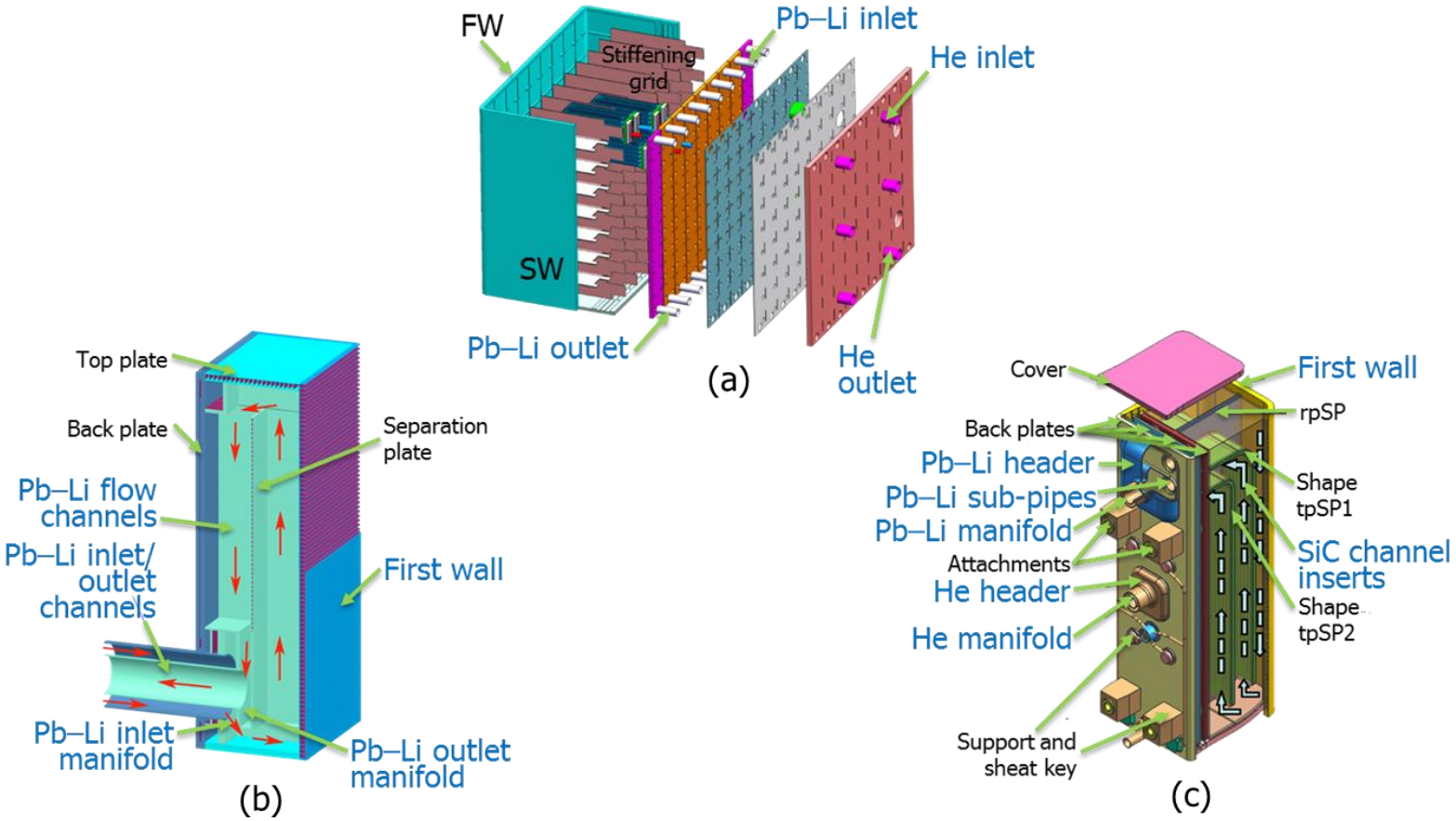


Figure 1.3 Test Blanket Module (a) HCLL, (b) DCLL and (c) DFLL.

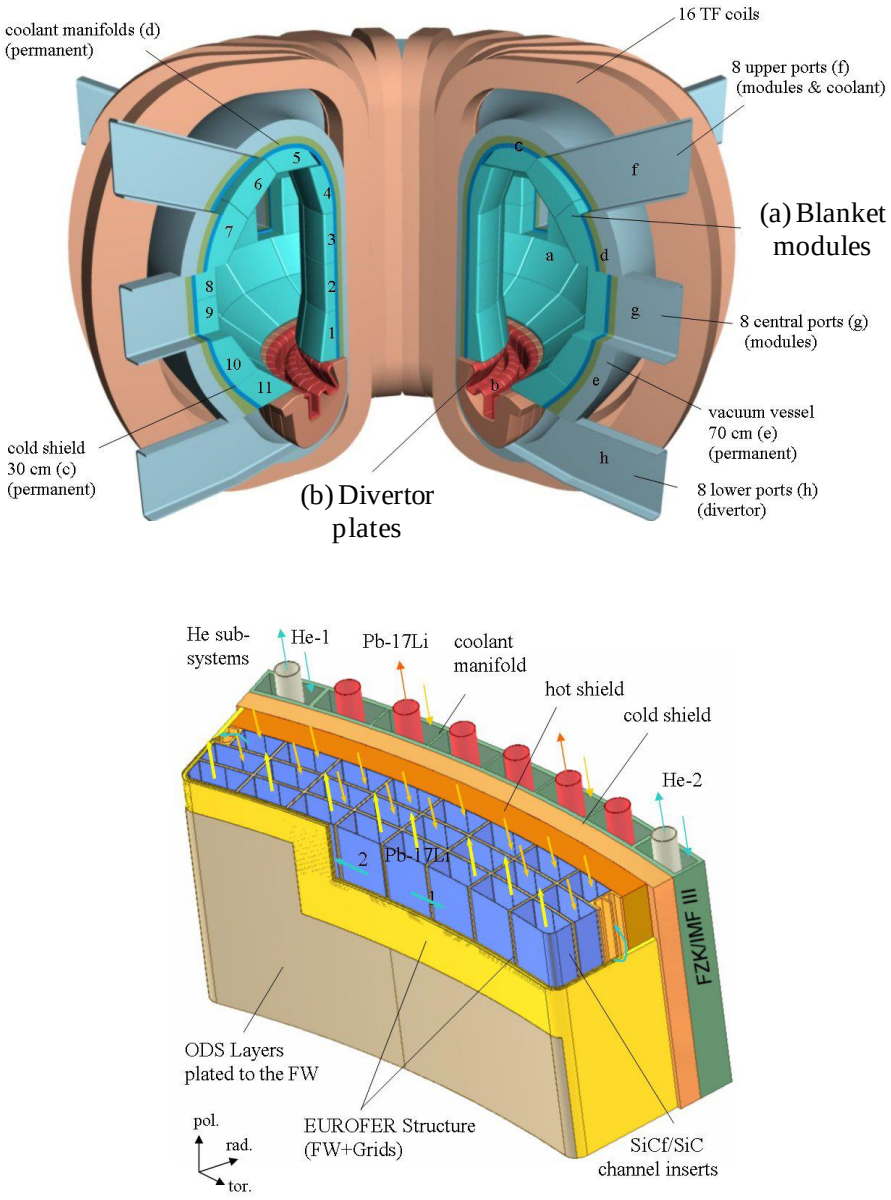


Figure 1.4 Schematics of dual coolant equatorial outboard blanket module in fusion reactor components [20, 21].

## 1.4. Candidate materials of components for nuclear reactor

### 1.4.1. Structural and/or functional materials of fusion reactor

The challenge is to develop structural materials which maintain high performance during prolonged exposure to high thermal and radiation flux. In addition to their structural properties, they may need chemical compatibility with coolants and be relatively easy to manufacture. The thermo-mechanical properties must not be degraded significantly due to damage and activation by 14 MeV neutrons. Heat conductivity should be maintained as well as low swelling and void formation, despite high levels of helium and hydrogen production. Weld-ability after irradiation should also be considered in order to allow re-welding after the maintenance operation. They should also have low levels of nuclear self-heating after irradiation and low activation to ease both maintenance and recycling of material. In the sixties and seventies the high temperature advantage of refractory alloys (based on molybdenum, tungsten, and vanadium) gave impetus to their development for fusion applications. Their major drawback was their embrittlement after irradiation. Therefore, in the late seventies attention shifted to low activation alloys and the development of vanadium-alloys was emphasized. Research work was started on reduced activation austenitic steels where elements with high neutron induced activation (like nickel) were replaced by elements (such as manganese) with similar overall properties, but low activation. These steels fell into disfavor due to their poor phase stability and the complexity of fabrication. In the early nineties the study of low activation ferritic-martensitic steels started. The track record of conventional chromium steels exposed to high neutron fluxes in fast breeder reactors encouraged the investigation of ferritic/martensitic steels including oxide dispersion strengthened ferritic/martensitic steels. The present decade has seen attention broaden to high temperature SiC/SiC composites. Some attention has been devoted recently to titanium and chromium alloys but these are still at an early stage of development.

### 1.4.2. The requirement for structure materials

The structural materials of first wall and blanket in DT tokamak reactor suffer from:

1) High surface heat flux causes mechanical and electromagnetic loading and alternating thermal stresses;

2) High energy (14.1 MeV) fusion neutrons produce displaced atoms and helium, hydrogen, and solid transmutation products, leading to changes in bulk properties.

The blanket systems are large systems with combined thermal, hydraulic and mechanical loading, irradiation, compatibility etc. The requirements for fusion structural materials are:

1) The material could withstand high neutron wall loads under temperatures and coolant pressure conditions necessary to drive efficient thermodynamic cycles in a blanket;

2) The lifetime of structural material must be long enough to minimize the necessary replacements of near-plasma components;

3) The material should be of low activation in order to achieve the ultimate environmental attractiveness of fusion power.

### 1.4.3. Candidate structural materials for blanket

#### 1.4.3.1. Reduced activation ferritic/martensitic (RAFM) steels

These alloys have the most advanced technological and industrial development due to the experience acquired in fossil and nuclear energy technology. They show reasonably good thermo-physical and mechanical properties, adequate resistance to radiation-induced swelling and helium embrittlement, and good compatibility with major cooling and breeder materials. Moreover, industrial batches have already been produced such as the F82H-mod. in Japan and the EUROFER 97 in Europe, and further studies towards super-clean steels are in progress. Development is required in several critical areas. Material with further reduced activation is needed, their radiation-induced hardening and embrittlement in a fusion relevant environment needs to be better understood. To enlarge their range of application to higher temperature, possible improvements using the technique of oxide dispersion strengthening is under investigation.

#### 1.4.3.2. Vanadium-based alloys

Vanadium-based alloys have moderate high temperature strength, adequate ductility above room temperature, and low long-term induced radioactivity. They show good resistance to high heat loads and allow high operational temperatures. The maximum operating temperature is limited by thermal creep while the low temperature limit is determined by irradiation hardening. A major drawback is the high solubility of interstitial elements like oxygen, nitrogen and carbon having the potential to lead to unacceptable embrittlement. Therefore measures have to be taken to control and prevent their pick-up during manufacture and operation.

#### 1.4.3.3. Fibre-reinforced composite materials based on silicon carbides

These materials have been conceived and developed mainly for aerospace applications and fossil power generation plants due to their potential for high temperature operation and high corrosion resistance which allows thermodynamic efficiency to be maximized. In addition for use in fusion, they exhibit very low short and medium term induced radioactivity and afterheat. The key issues to be addressed include the irradiation performance, the scaling up of fabrication techniques for large components, the lack of suitable techniques for joining parts since welding is not possible, the effect of matrix porosity and micro-cracking on coolant hermetic sealing capacity, the need for standardization and (at present) the high cost.

(1) The NITE–SiC/SiC composites

The matrix cracking stress of fibrous ceramic composites is determined by the matrix porosity (through fracture energy and effective modulus effects) and fiber–matrix interfacial strength, in an ideal condition, when elastic moduli for the fiber and matrix are similar. In fact the tensile proportional limit stress of SiC/SiC composites tends to negatively correlate with the matrix porosity. Porosity reduction is also essential for maximizing the composite's thermal conductivity for given inherent thermal conductivity of the constituents. 'Strong' fiber–matrix interfaces, in contrast to conventional 'weak' interfaces for fibrous ceramic composites, are beneficial not only to the matrix cracking strength but to the toughness, the lifetime and the creep resistance. The NITE–SiC/SiC composite was developed for the reduced porosity, advanced matrix quality control and strong fiber–matrix interface [22].

The NITE process incorporates an appropriate coating to the fiber surfaces for the fiber protection and the interphase deposition, infiltration of nano-phase SiC powder-based mixed slurry to the coated fiber preform, and a pressure sintering of the matrix at a temperature slightly above melting point of the transient eutectic phase. The optimized combination of the fiber coating condition, the matrix slurry condition and the sintering condition results in the quality matrices (with small porosity, appropriate SiC grain sizes, acceptable amount of oxide remnants in desired phases) and an acceptable amount of fiber damage. A detailed description of the basic process is found elsewhere [23].

The microstructures, fast fracture strength properties at ambient temperature, and some thermo-physical properties have been studied. Representative properties of the lab-grade NITE–$SiC_f$/SiC composites are presented in Table 1.6, apparently meeting most property values suggested by international reviewers for design analysis of SiC/SiC-based power plants for the long term. The thermal conductivity of NITE–SiC/SiC composites shown in Table 1.6 is for an unirradiated condition and should undergo a significant reduction after neutron irradiation depending on temperature. The magnitude of primary thermal resistance of NITE–SiC/SiC, which comes from grain boundaries and impurities, will probably be comparable with the anticipated thermal resistance added by neutron irradiation in most fusion conditions. Therefore, improving the unirradiated thermal conductivity should significantly improve the irradiated thermal conductivity.

Table 1.6 Representative properties of NITE–SiC/SiC as compared with those suggested for analysis of SiC/SiC-based power plants for the long term [22].

| Key SiC/SiC properties | Suggested value | NITE (lab grade) |
|---|---|---|
| Density | ~3000 kg/$m^3$ | 2800–3000 kg/$m^3$ |
| Porosity | ~5% | 3–6% |
| Young's modulus | 200–300 GPa | 190–220 GPa |
| Thermal expansion coefficient | $4 \times 10^{-6}$ $K^{-1}$ | $3.3–4.7 \times 10^{-6}$ $K^{-1}$ (20–1000°C) |
| Thermal conductivity through thickness | ~20 W/m K | 17–29 W/m K (20°C) [1)]<br>15–20 W/m K (1000°C) [1)] |
| Maximum allowable combined stress | ~190 MPa | ~150 MPa [2)] |
| Cost | < $400/kg | ~$5000/kg [3)] |

[1)] Unirradiated. [2)] 2/3 of tensile proportional limit stress. [3)] Rough estimate for a 10 kg batch of cross-plied composite.

Table 1.7 Proposed ITER test module.

| TBM | Country | Structure materials | Breeder | Multiplier | Coolant |
|---|---|---|---|---|---|
| HCSB | US, EU, Japan, China, Korea, RF | F82H or EUROFER | $Li_4SiO_4$ or $Li_2TiO_3$ | Be or $Be_{12}Ti$ (pebbles) | He |
| WCSB | Japan | F82H | $Li_2TiO_3$ or others | Be or $Be_{12}Ti$ (pebbles) | $H_2O$ |
| DFLL | China | CLAM | Pb–17Li | – | He |
| HCLL | EU | EUROFER | Pb–17Li | – | He |
| DCLL | US | F82H | Pb–17Li | – | He |
| HCML | Korea | EUROFER | Li | – | He |
| SCLi | RF | V–4Cr–4Ti | Li | Be | – |

# 2. Fundamentals of compatibility studies of advanced material with liquid Pb–Li for HT blanket system

## 2.1. The biomass-fusion hybrid concept

Hydrogen is considered as the most potential energy carrier in the near future and can be produced from nuclear energy by several means. Biomass is one of the sustainable energy resources. Human beings are having been relying on biomass resources, in particular, woody biomass. Wood can be used as structural materials or fuels as it is. Some other biomass resources, for example, algae, cones, and raw garbage are expected as potential energy source in near future. In a view of $CO_2$ emission, these resources are regarded as "Carbon neutral" because $CO_2$ gas emitted from these fuels are originally absorbed by the biomass from the atmosphere. Although these biomass resources are valuable as it is, economical values of these resources can be higher if processed in a correct fashion. As mentioned in the previous section, hydrogen fuels or synthetic oils can be produced by the gasification of these biomass resources. Typical gasification reaction of cellulose is described as [19];

$$(C_6H_{12}O_5)n + H_2O \rightarrow 6nH_2 + 6nCO - 816n\ kJ\ (Cellulose) \quad (1.2)$$

In addition, if the produced hydrogen and carbon monoxide processed farther to produce more hydrogen fuels or synthetic oils as;

$$CO + H_2O \rightarrow H_2 + CO_2 + 32\ kJ\ (Shift\ reaction) \quad (1.3)$$

$$2H_2 + CO \rightarrow -CH_2- + H_2O + 160\ kJ\ (Fischer\text{-}Tropsch\ reaction) \quad (1.4)$$

Created oil can be used for the fuels of automobiles and airplanes.

This process is quite attractive for many countries where no major mines of fossil fuels are available. Any country can produce oil in their lands through these processes. However, the gasification of biomass requests large amounts of heat. Plus, high temperature heat (> 900℃) is required in order to achieve high gasification efficiency. Here, the nuclear fusion plant can work as the high temperature heat source. Liquid metal coolants considered for the blanket and divertor cooling can be heated to > 900℃. For the high temperature structure or insulator panels, SiC/SiC composites withstand high temperature operation. Thus, the fusion nuclear heat can be obtained at the high temperature and applied to the gasification process.

If other hydrogen energy related technologies, such as transport and storage, are developed, this fusion-biomass hybrid plant can work as the hydrogen production plant. Hydrogen fuels produced from this plant can be used for the fuel cells, hydrogen gas turbines, or other combined power generation systems. The strong advantage of this concept over the normal fusion power plant is the application to the load following operations. Since the fusion power is not easily controlled to follow the requirements, the use of normal fusion power plant is limited to the base-load operation where many other options with higher energy efficiencies are available. However, fuels produced from the fusion biomass hybrid plant can be used for the load follow operations where higher cost than the base load operations are acceptable.

## 2.2. R&D needs for the HT blanket systems

The high temperature blanket is desirable for hydrogen production, but some R&D needs should be specified, such as tritium permeation and chemical compatibility under high temperature and under irradiation, and coating technology to avoid inter-contamination issues between hydrogen production system and fusion reactor system [19].

SiC/SiC composites have been developed for aerospace applications and fossil power generation plants because of their high temperature strength, strength to weight ratio and high corrosion resistance. The application of SiC/SiC composites as materials for blanket structural and/or functional component can significantly increase the upper operation temperature with the advantage of high thermodynamic efficiency. The structural and/or functional materials made of SiC/SiC composites, such as cooling panel and FCIs should be considered in the He and Pb–Li coolant channels besides in the heat exchangers to reduce tritium permeation into hydrogen production system, and vice versa, to reduce hydrogen permeation into blanket coolant system. The compatibility of SiC/SiC composites is a concern for the high temperature Pb–Li blankets.

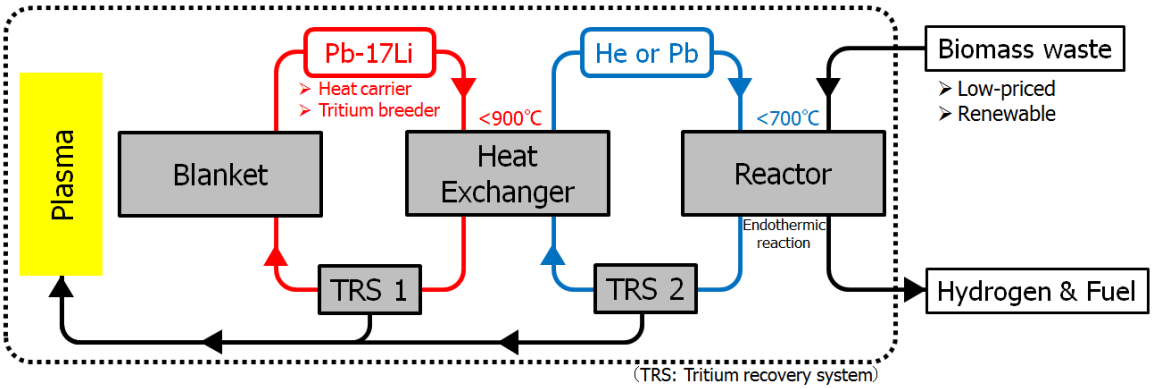


Figure 2.1 The High Temperature blanket system for fuel production.

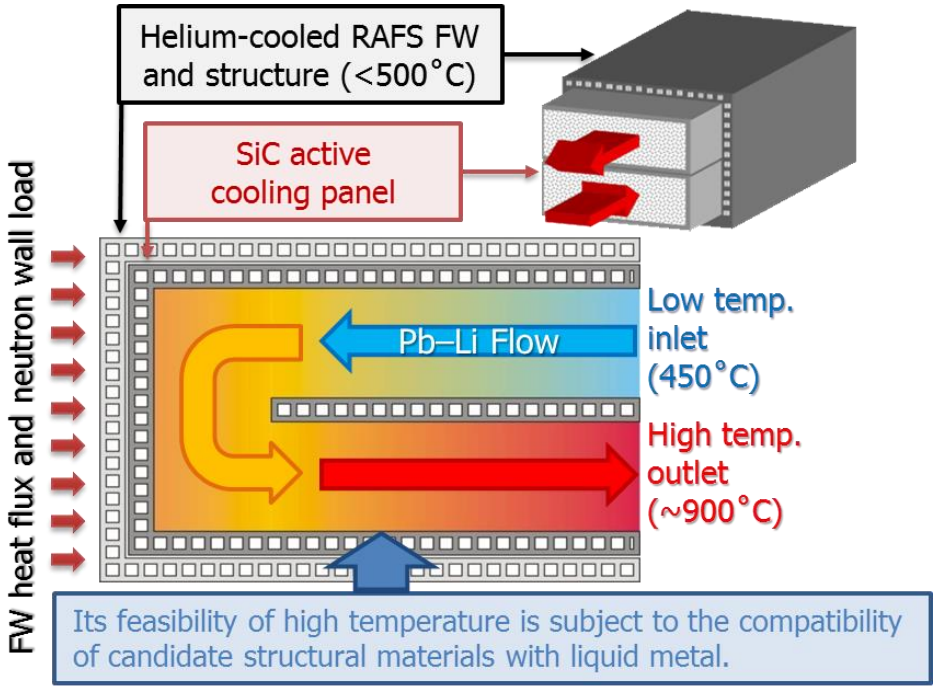


Figure 2.2 Simplified Pb–Li/SiC blanket module flow scheme.

The compatibility evaluation technologies need to be studied and developed in this thesis. It is needed to have good compatibility with fundamental material and high temperature Pb–Li, to achieve low T-permeation rate and to provide self-healing function on defects that might occur in normal operation or accidental conditions. Figure 2.2 shows simplified Pb–Li/SiC blanket module flow scheme. This concept blanket system is operated as high temperature. Technology development is more required for intermediate heat exchanger due to large area and thin wall for efficient heat transfer from the primary coolant Pb–Li to the secondary system. The chemical compatibility of Pb–Li and SiC/SiC at high temperature is an area in need of R&D for

high temperature Pb–Li blanket. The compatibility problem is more serious under the high temperature and high flowing velocity of Pb–Li. Only limited data on the compatibility of SiC/SiC with Pb–Li are available.

## 2.3. Problem of compatibility analysis

The classification of techniques for compatibility evaluation can be classified as shown in Table 2.1. In consideration of technique characteristics of compatibility evaluation with liquid metal, evaluation techniques are contributed to be limited to these three methods, static pot, thermal convection loop, forced convection loop and electrochemical cell.

The compatibility of materials in lithium–lead with flowing condition is different mechanism from static condition, and the corrosion quantity is thereby big and different. These reasons include what erosion/corrosion are easy to produce for the corrosion of the elution type being easy to occur than liquid metal lithium which I described in [24, 25], specific gravity of lead lithium that, besides, nearly 20 times is bigger than lithium.

Table 2.1 Classification of techniques for compatibility evaluation.

| Name | Objective & characteristic | Parameter control | | |
|---|---|---|---|---|
| | | Flowing | Temperature gradient | Electrochemistry |
| Static pot | - saturated condition<br>- surface corrosion trend<br>- easy handling, compact<br>- possible of changed pot | × | × | ○ |
| Thermal convection loop | - unsaturated condition corrosion<br>- easy handling, complicate<br>- mass transport evaluation | △ | ○ | △ |
| Forced convection loop | - difficult handling, complicate<br>- unsaturated condition corrosion<br>- erosion-corrosion<br>- flow-accelerated corrosion<br>- mass transport evaluation | ○ | ○ | △ |
| Electrochemical cell | - electrochemical corrosion<br>- corrosion potential measurement | × | × | ○ |

## 2.4. Research status of compatibility of advanced materials with liquid metal Pb–Li

Liquid lithium–lead alloy is regarded as an attractive breeding material because of is high tritium breeding rate, high thermal conductivity and so on. Pb-Li intending for here is 83% of molar fractions of the Pb, composition of 17% of molar fractions of the Li, and the melting point is lowest 235℃ among lithium-lead alloys, as shown Table 2.2.

Table 2.2 The properties of liquid metal breeder.

| Candidate | Li | Pb–Li | Flibe ($2LiF–BeF_2$) |
|---|---|---|---|
| Density ($g/cm^3$) | 0.48 | 9.0 | 2.0 |
| Heat conductivity ratio (W/m/K) | 42 | 14 | 1 |
| Melting point (K) | 453 | 508 | 732 |
| Thermal capability (J/g/K) | 0.50 | 0.17 | 2.3 |
| Resistance (Ω cm) | $2.9\times10^{-5}$ | $1.3\times10^{-4}$ | 0.65 |
| Reaction with water | Strong reaction | Reaction | No reaction |
| Tritium recycle | Difficult | Easy | Difficult (TF), Easy (HT) |
| Tritium inventory | High | Low | Easy (HT), Difficult (TF) |
| MHD concern | High (self-cooled) | Normal | Low |

Several studies have been conducted to evaluate the influence of material and system parameters on the corrosion behavior of austenitic, ferritic steels, and SiC ceramics in liquid metal Pb–Li environment. The principal mechanisms of corrosion of materials in a liquid metal environment are dissolution, inter-granular penetration, interstitial-element transfer, and mass transfer due to thermal and concentration gradients.

About compatibility on materials in liquid metal Pb–Li, it has been already reported a lot in the 1980s. A lot of data of the corrosion of the austenite steel are written in the review article at that time by Dr. Coen, because 316 types of austenite steel became the first wall candidate materials [26]. However, the corrosion of the ferrite steel begins to be checked from this time. In Oak Ridge National Laboratory, U.S.A., they researched corrosion of the ferrite steel (mainly HT-9 of 12Cr) using both natural convection loop and forced convection loop. They carried out a corrosion experiment under conditions of comparative low temperature to 538℃, and the Chopra doctors clarified temperature in the low temperature and influence of the velocity using a forced convection loop of Pb–Li of 2 liters [27-29]. In addition, in Europe, results of research are given at this time. Tas doctors installed a thermal convection loop of 316 types of austenite steel (LELI) to ferrite steel (1.4914 steel: Fe–10.6Cr) and carried out an examination of

long duration test as many as 5455 hours [30]. In France Tulip thermal convection loop (product made in ferrite, Pb-Li inventory: 1 liter approximately) examination of around 3000 hours is implemented [31] In these studies, it is checked the material transportation other than the corrosion of the specimen, and, in loops with the difference of temperature, that the deposition of low-temperature precipitation and the dissolution corrosion of high-temperature precipitation occurs at the same time has been revealed. By a study of the 1980s, lithium lead and the tendency of the corrosion reaction of steel materials became clear mainly. When the 1990s begins, the influence such as impurities of lithium lead is discussed [32], also experiments [33] and discussion [34] about the impact against corrosion of the magnetic field that indispensable to blanket has also been reported as paper further, but since the influence of purity maintenance of Pb–Li to corrosion is large, the effect of the magnetic field (1.4T perpendicular to a flow) is not clarified. In recent study, there are report on ferrite steel was immersed in high temperature conditions of 700℃ or more as a background dual cool type of He and Pb–Li, and also the co-existence of the corrosion-resistant coating [35]. In addition, result about the flow acceleration corrosion of the ferrite steel which is examined by a loop named PICOLO from the German Karlsruhe Institute is reported [36, 37]. Moreover, in China, a thermal convection loop named Dragon and forced convection loops are produced, and the result of the corrosion examination has begun to be reported [38].

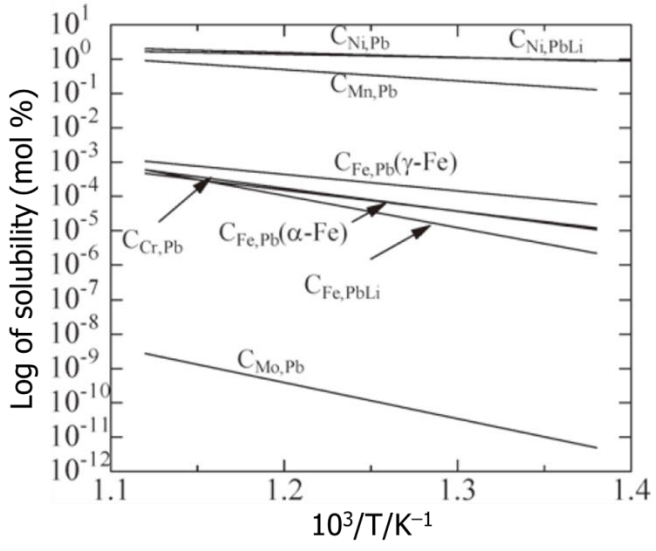


Figure 2.3 The solubility of metallic elements in liquid metal Pb–17Li [39].

### 2.4.1. Compatibility of RAFM with Pb–Li

Studies were carried out on compatibility of RAFM steels with flowing Pb–Li. The past data are summarized in Table 2.3 [36, 40-42]. At 480℃, the evaluated corrosion rate of RAFM steels is less than 100 μm/yr in Pb–Li, although the test periods changed from 4500–12000 h. It indicates that the weight loss of RAFM increases linearly with the exposure time. It should be noticed the corrosion rate significantly increases with increasing the test temperature: 700 μm/yr at 550℃ [41]. As for the flow rate effect, high flow rates resulted in a high corrosion rate, indicating that the flow rate needs to be suppressed to reduce the corrosion rate.

It was reported that it took time for Pb–Li alloy to wet whole surface of specimen during exposure. The wetting issue could result in an apparent low corrosion rate at the first stage of experiment because the corrosion might only occur in the section where the steels contacted with Pb–Li. The period of wetting depends on the temperature [40] and surface condition of specimen, such as original oxide layer [43]. Figure 2.4(a) and (b) shows the metallographic observations of EUROFER 97 after typical corrosive Pb–Li attack for different exposure time. As shown in Figure 2.4(a), the surface of sample was all covered with the Pb–Li alloy after exposure for 1500 h. In Figure 2.4(b), the SEM micrographs obtained on the cross-section of the 3000 h tested samples are reported. As presented in the figures, a layer about 1 μm thick seems to detach from the surface of the steel. At the interface between the layer and the bulk material, voids could be observed, and the EDX analysis indicated that the layer was Cr depleted. The experiment in other system also proves that the dissolution of Cr and Fe from RAFM in Pb–Li is the major mechanism.

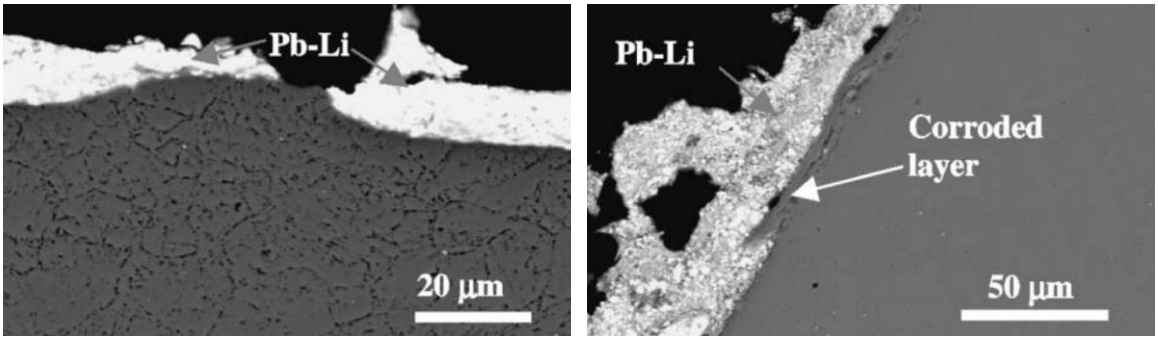


Figure 2.4 Cross-section of EUROFER 97 after exposure in Pb–Li [42].

The corrosion of different RAFM in Pb–Li was compared by Konys [41]. A summary of the maximal corrosion attack result from MANET I, OPTIFER Iva, F82H-mod., EUROFER 97 and SiC ceramics was given in Figure 2.4. The lines for each alloy type were

inserted by optical fitting to illustrate the time dependency. According to figure, the corrosion line of EUROFER 97 is 10–20% lower than other RAFM steels. This cannot be explained by the chemical dissolution of alloy elements, because these alloys have very similar alloy composition. Probably the minor alloy elements, such as Ti and N, or low impurity level in steel are responsible for the difference. It is also influenced by initial oxide layer on the surface of specimens. It was reported that the initial oxide layer delayed the onset of corrosion [43].

Table 2.3 Corrosion rate of advanced materials in the Pb–Li.

| Material | Material of crucible & pipe | Method, Flow regime/ B field | Temperature, $T_{max}$ (℃) | Flow rate (m/s) | Exposure time (h) | Estimated corrosion depth (μm/yr) | Ref. |
|---|---|---|---|---|---|---|---|
| Martensitic steel Ferritic steel (26%Cr) | | Static | 440-500 | | 500 | | [44] |
| Austenitic materials | | | | | | | [45] |
| Fe–12Cr–1MoVW | | Flowing (laminar) | 500 | | | 24 | [46] |
| HT-9, Fe-9CR | | Flowing (laminar) | 482 | | | 20 | [47] |
| 1.4914 | | Flowing (turbulent) | 550 | | | 370 | [48] |
| | | Flowing (turbulent) | 475 | | | 40 | [49] |
| 1.4914 | | Flowing (laminar) | 450 | | | 30 | [31] |
| EUROFER 97 | | Flowing (laminar) | 480 | 0.3 | 12000 | 90 | [40] |
| | | Flowing (laminar) | 550 | 0.3 | 1000 | 700 | [41] |
| | | Flowing (laminar) | 480 | 0.01 | 4500 | 40 | [42] |
| EUROFER | | Flowing (laminar) | 550 | | | 237–530 | [50] |
| | | Flowing (laminar)/ 1.7 T | 550 | | | 550–900 | [50] |
| EUROFER | | Flowing (turbulent) | 480 | | | 90 | [37] |
| OPTIFER Iva, F82H-mod. | | Flowing (turbulent) | 550 | | | 400 | [37] |
| OPTIFER, MANET 1, F82H-mod. | | Flowing (laminar) | 480 | 0.3 | 6000 | 100 | [36] |
| | | Flowing (turbulent) | 480 | | | 100 | [36] |
| JLF-1 {Re number} | F2–9Cr | Flowing | 600 | {18512} | 250 | | [51] |
| | JLF-1 | Static | 600 | – | 500, 750, 3000 | | [25] |

## 2.5. Objectives of this research

As described above, SiC and SiC/SiC materials are promising candidate for structural and/or functional materials of high temperature Pb-Li blanket system, because of excellent elevated temperature strength, corrosion resistance, electrical insulation and irradiation resistance in nuclear environments. In order to carry out research reproduced the flowing condition at high temperature, and to acquire the engineering database and scientific understanding required for the basic design of high temperature Pb–Li blanket system, the compatibility problems on advanced SiC materials with flowing of high temperature Pb–Li blanket system were investigated and evaluated.

Chapter 1 and 2 here, the backgrounds were overviewed on R&D of advanced nuclear systems and advanced SiC ceramic materials. The influence of the different experimental parameters, such as a flowing condition, an exposure time and a geometric condition, on the corrosion behavior was investigated. In Chapter 3, compatibility evaluation technology which reproduced the flowing condition at high temperature i.e. rotating disk system has been introduced and improved. In Chapter 4, the compatibility of advanced SiC ceramic materials exposed to liquid Pb–Li at high temperature has been investigated by the rotating disk system with flowing condition. The formation mechanism on surface of SiC materials in high temperature Pb–Li blanket system was evaluated. And that's rule factor is clarified by microstructural analysis. Based on the results in previous chapters, Chaper 5 deals with assessment of feasibility for the functional applications of advanced SiC ceramic materials to blanket system, such as cooling panel and FCI with electrical conductivity and insulation. Summary and conclusion will be finalized in Chapter 6.

# 3. Development of technique on compatibility evaluation for high temperature

## 3.1. Introduction

Liquid lithium–lead blankets have attracted attention in design concepts such as the Helium-Cooled Lithium Lead (HCLL) in EU, the Dual Coolant Lithium Lead (DCLL) in US, and the Dual-Functional Lithium Lead (DFLL) in China because of the promising advantages for future fusion power reactors [52-56]. The DCLL blanket has a low activation ferritic steel structural material, and a SiC flow channel insert [38, 57-59]. The authors proposed using cooling panels made of SiC/SiC composites to actively control the heat flux to achieve Pb–Li temperatures exceeding 900℃. This concept drastically improved the total energy efficiency and also enables other attractive applications such as hydrogen production [60]. For the feasibility of this concept, the compatibility of SiC with liquid Pb–Li at 900℃ is important [35, 61-63].

There are some issues with the compatibility of liquid Pb–Li with other system materials, particularly related to flow rates. Many components of the materials in contact with the liquid have some limited solubility. For static conditions [62], dissolution of that material is expected to stop when the solubility limit in the liquid is reached. However, for flowing conditions when the solute density in the liquid is lower than solubility, the continuing corrosion occurs. This corrosion rate is influenced by the relative velocity of the flowing liquid at the surface of the material. In order to measure the corrosion or erosion by liquid metals during flow conditions, a simple apparatus was developed. The rotating disk (RD) system can expose samples with the wider range of parameters such as relative flow velocity, temperature and chemical environment compared with static corrosion test. We used the RD system to evaluate the corrosion behavior as a function of contact velocity between SUS316 steel and Pb–Li at 500℃ for 500 h, and observed the change of the surface of the specimens. Then, the test by using RD system made of molybdenum carried out to evaluate the compatibility behavior on NITE (Nano-Infiltration Transient-Eutectic-Phase) SiC/SiC composites [23] in Pb–Li at 900℃ for 1000 h.

It was reported that the dissolution of an oxide layer formed on the materials surface in water was accelerated at a flowing condition, and the phenomenon was called as flow-accelerated corrosion (FAC). It was known that the corrosion mechanism in the liquid breeders is the dissolution of the matrix elements in the fluids [64, 65]. Also in the liquid metals and molten salts, the FAC phenomena for the dissolution of the steel surface can be caused by the promotion of the diffusion in

the corrosion process. An erosion of a corroded surface by the shear stress of the flow called an erosion–corrosion [66] is also an important phenomenon for the liquid breeders. However, the information in liquid metals and molten salts are limited so far.

Therefore, there are some issues with the compatibility of liquid Pb–Li with other system materials, particularly related to flow rates. Many components of the materials in contact with the liquid have some limited solubility. For static conditions [62], dissolution of that material is expected to stop when the solubility limit in the liquid is reached. However, for flowing conditions when the solute density in the liquid is lower than solubility, the continuing corrosion occurs. This corrosion rate is influenced by the relative velocity of the flowing liquid metal at the surface of the material.

In the present study, two types of simple assembles, Rotating Disk (RD) systems, were developed and estimated to measure the phenomenon of compatibility by liquid metals even at high temperature during flowing conditions. The compatibility of SUS316 and NITE–SiC/SiC composites in the liquid breeders with a flowing condition by these rotating disk systems was investigated by means of corrosion tests by two types of RD systems. The influence of the different experimental parameters, such as a flowing condition, an exposure time, a geometric condition and a chemical environment, on the formation behavior on compatibility was investigated for HT blanket model.

## 3.2. NITE–SiC/SiC composite in forced convection loop

Figure 3.2 shows result by using forced convection loop (Figure 3.1) at Kyoto university. The experiment by using this loop can provide various data with the reciprocity than static pot and thermal convection loop. However, it is a large complex form with various devices for operating. And the change of container materials is severe. Safety is important for experiments prolonged at high temperature. The Fe and Cr eluted from the region except the examination department attach on the surface of the specimen of the testing part. For reproduced flowing condition at high temperature, the quantitative evaluation method that high in integrity is required.

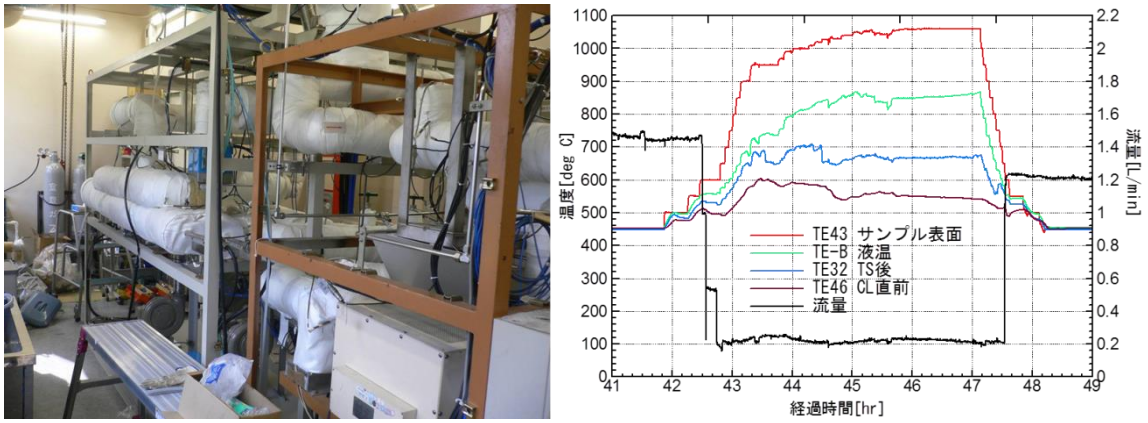


Figure 3.1 Experiment of NITE–SiC/SiC composite in forced convection loop (@ Kyoto university).

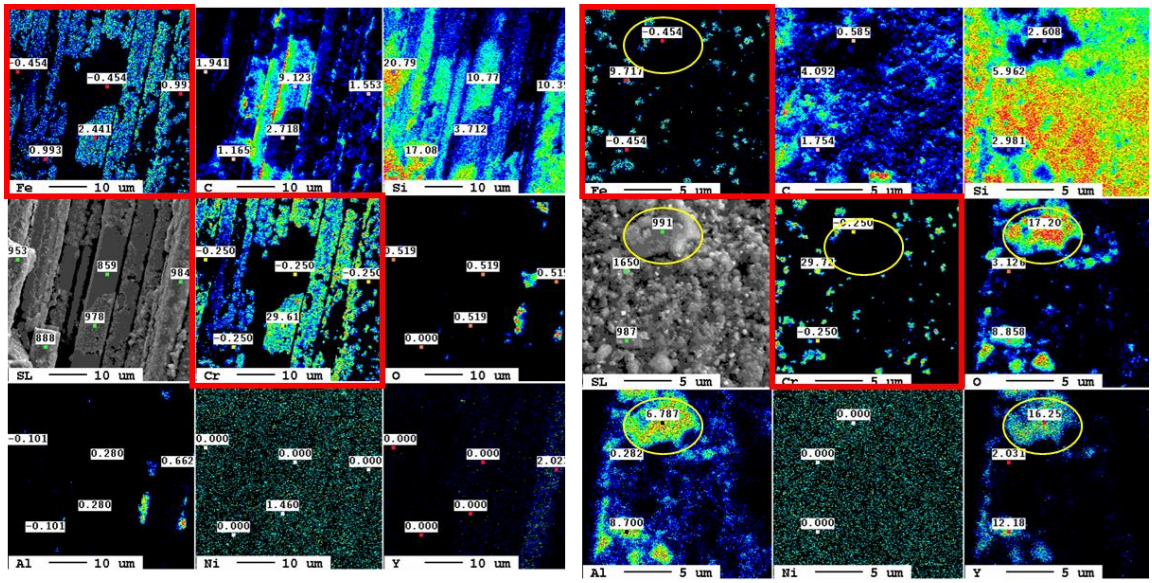


(a) Part of SiC fiber (b) Part of NITE matrix

Figure 3.2 EPMA evaluation of the surface on NITE–SiC/SiC composite in forced convection loop at 700C for 2 weeks (about 336 h).

## 3.3. Rotating disk systems with flowing condition at high temperature

The tests in a Pb–Li test were performed using crucibles made of pure alumina (before improvement) and pure molybdenum (after improvement), respectively, with specimen holders made of the same material as the crucible. Except for the Mo, the crucible and holder materials could also corrode and may influence the corrosion of the specimens. The Pb–Li flow in the pot is induced by a rotating disk specimen. There was no baffle plate to decrease the rotating flow, and the pot was

referred to as the RD system [67, 68]. The rotating Pb–Li flow included only small upward and downward flow components produced by the rotating disk specimen, so the Pb–Li is well mixed with near constant concentration of impurities throughout the liquid volume. The RD system (Figure 3.3) was designed to investigate the effects of flow conditions on the corrosion without any temperature gradient. Flow velocities higher than in the thermal convection loop can be reached in this system.

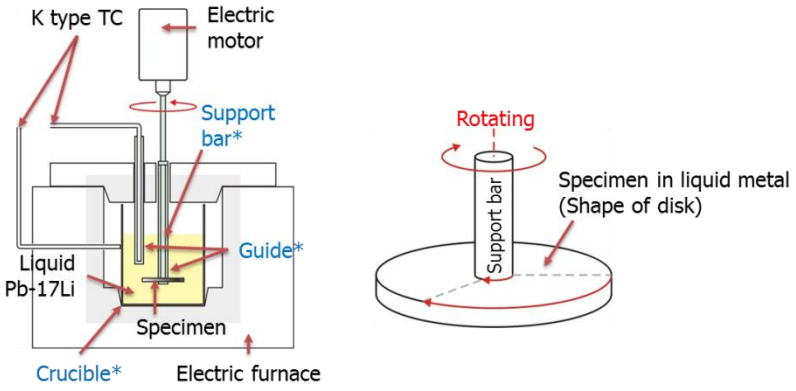


Figure 3.3 Schematic diagram of rotating disk system.

The rotating disk system was designed to investigate the effect of flow conditions on the corrosion without temperature gradient. The flow velocity for the test is higher than the velocity in the thermal convection loop. The pot was assembled in a glove box covered with 99.999% Ar. The flow may influence the corrosion as the diffusion of the element dissolved from the specimen surface is promoted, and the shear stress works on the specimen surface which can cause erosion/corrosion. Table 3.1 shows comparison with classification of techniques for compatibility evaluation.

Table 3.1 Comparison with classification of techniques for compatibility evaluation.

| Name | Objective & characteristic | Parameter control | | |
|---|---|---|---|---|
| | | Flowing | Temperature gradient | Electrochemistry |
| Static pot | - saturated condition<br>- surface corrosion trend<br>- easy handling, compact<br>- possible of changed pot | × | × | ○ |
| Thermal convection loop | - unsaturated condition corrosion<br>- easy handling, complicate<br>- mass transport evaluation | △ | ○ | △ |
| Forced convection pot | - easy handling, compact<br>- unsaturated condition corrosion<br>- erosion-corrosion<br>- flow-accelerated corrosion<br>- mass transport evaluation | ○ | △ | ○ |

| | | | | |
|---|---|---|---|---|
| Forced convection loop | - difficult handling, complicate<br>- unsaturated condition corrosion<br>- erosion-corrosion<br>- flow-accelerated corrosion<br>- mass transport evaluation | ○ | ○ | △ |
| Electrochemical cell | - electrochemical corrosion<br>- corrosion potential measurement | × | × | ○ |

## 3.4. Experimental procedure

### 3.4.1. Experimental apparatus

An apparatus to rotate disk materials in a liquid metal was used to measure the effect of flow speed as a function of the radial position on the disk. This rotating apparatus, represented in Figure 3.3 and Figure 3.4, consisting of the electric furnace, the crucible with panels, the support rod with guide, thermocouple and electric motor, was placed in a glove box containing a high purity argon gas, and the atmosphere was controlled at $O_2$ < 0.01 ppm and moisture < 0.1 ppm. Two types of experimental devices were used to isolate the effects of flow on the compatibility. A disk sample was mounted on the support rod and was immersed in the crucible containing liquid metal. The disk was rotated and exposed to the flow with various relative speeds. The crucible contained about 1.5 kg of Pb–Li and was heated to the temperature range (~900℃) by the electric furnace. The temperature was measured and controlled with type K thermocouples contained in a central molybdenum tube. All materials for the crucible, support rod, thermocouple protection tube, etc. that contacted liquid Pb–Li were alumina and molybdenum which was expected and reported to be compatible with lithium–lead alloy [61, 62, 69].

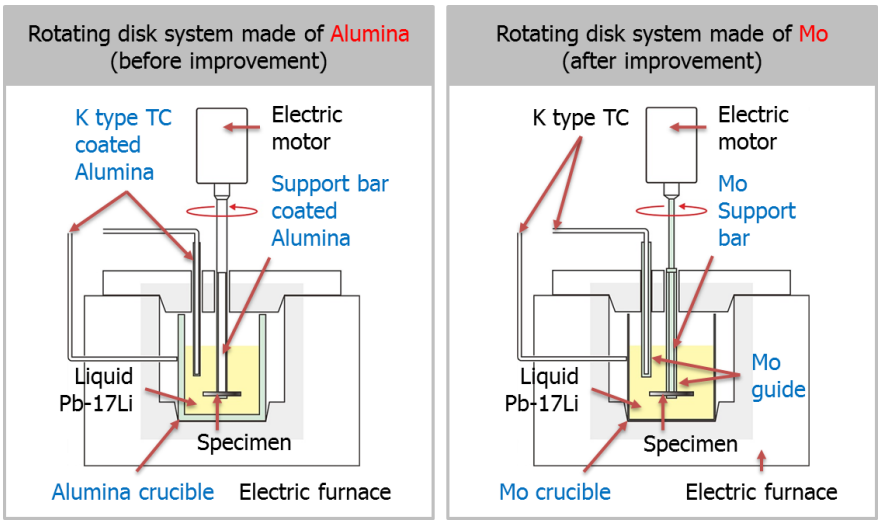


Figure 3.4 Two types of rotating disk systems in glove box (OMNI-LAB, VAC co.).

### 3.4.1. Sample and operating condition

The materials used in this study was SiC/SiC composites produced by the NITE process [22, 60] with SUS316 also included for reference. The composite contains the SiC fiber (Tyranno-SA 3rd, Ube Ind.) coated with C (thickness of the carbon interface was 200–300 nm). Density of the NITE–SiC/SiC was 3.01 g/cm$^3$. The specimens were shaped to disks of 30 and 35 mm diameter, 2 mm thickness. Before testing, the SUS316 specimen was cleaned in an alcohol–acetone mixture and the surface was lightly polished with a grinding paper (2400 grade) in order to eliminate the superficial oxide layer. However, in liquid metal, poor wetting of the stainless steel was observed when immersed, which could be due to incomplete removal of the superficial oxide layer. After the exposure in the Pb–Li, the specimens were immersed in an acetic acid–hydrogen peroxide–alcohol mixture (1/3:1/3:1/3) at RT (25℃) until the specimen weight reached a constant value by the removal of adhered Pb–Li from the surfaces of specimens [69]. The operating conditions of the apparatuses are shown in Table 3.4. The rotation speed of the support rod was about 200 rpm. The equivalent flow velocity is a function of radial position on the disk and ranged ~13.6 to 31.4 cm/s. The changes of appearance and chemical composition of the surface were analyzed and examined by optical microscopy, scanning electron microscopy installed in energy dispersive X-ray analysis, fluorescent X-ray observation and electron probe X-ray microanalysis before and after the corrosion experiment.

Table 3.2 Chemical composition of the samples in weight percent (Fe in balance).

| Material | Element | | | | | | | | | |
|---|---|---|---|---|---|---|---|---|---|---|
| | C | Si | Mn | Cr | Ni | P | Mo | V | W | Ti |
| SUS316 | 0.019 | 0.78 | 1.4 | 17–18 | 12.08 | 0.037 | 2.04 | – | – | – |

Table 3.3 Rotating disk systems.

| RD system | Crucible | Support bar | TC guide | Specimen diameter |
|---|---|---|---|---|
| Alumina system (before improvement) | Alumina | Type 316 SS coated alumina | Coated alumina | > 30 mm |
| Molybdenum system (after improvement) | Pure molybdenum[1)] | Pure molybdenum | Pure molybdenum | > 50 mm |

1) 99.95%, Nilaco, co.

Table 3.4 Experimental conditions of corrosion test in liquid Pb–Li.

| Material | SUS316 | NITE-SiC/SiC composite | | |
|---|---|---|---|---|
| RD system | Alumina | Alumina | Pure Mo | Pure Mo |
| Temperature (℃) | 500 | 850 | 900 | 900 |
| Exposure time (h) | 500 | 1000 | 1000 | 1000 |
| Diameter (mm) | 30 | 30 | 30 | 35 |
| Relative flow velocity (cm/s) | 13.6-31.4 | 13.6-31.4 | 10.5-31.4 | 10.5-36.6 |

## 3.5. Result and discussion

### 3.5.1. SUS316 and NITE–SiC/SiC composite in RD system made of alumina

Rotating flow velocity on liquid metal was measured by visualization experiment of acrylic container used water such as Figure 3.5. Because water and liquid Pb–Li have a similar material property in dimensionless number, in order to evaluate the flow of the disk surface in RD system, an imitation container is manufactured by ref. [70] , and the flow velocity is surveyed with the laser sensing fluid visualization measuring device by the PIV (particle image velocimetry) technique. Compatibility with an actual phenomenon was measured by the numerical fluid simulation and fluid visualization experiment. The Figure 3.6 shows the down of about 10% on the rotating flow velocity (value of flow velocity caused by diameter < about 10%).

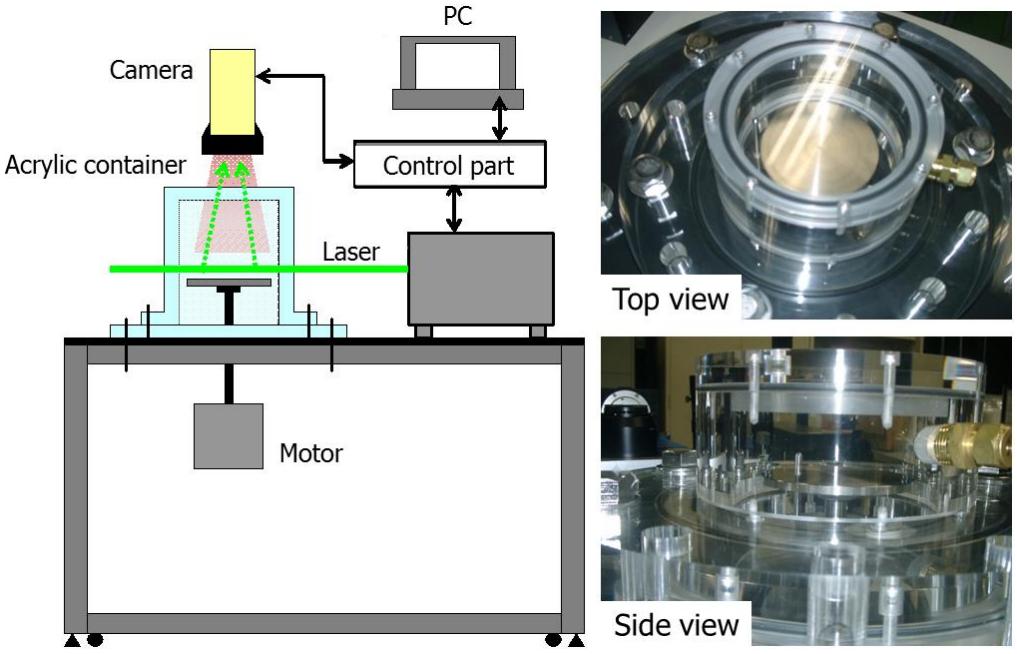


Figure 3.5 The laser sensing fluid visualization measuring device [71].

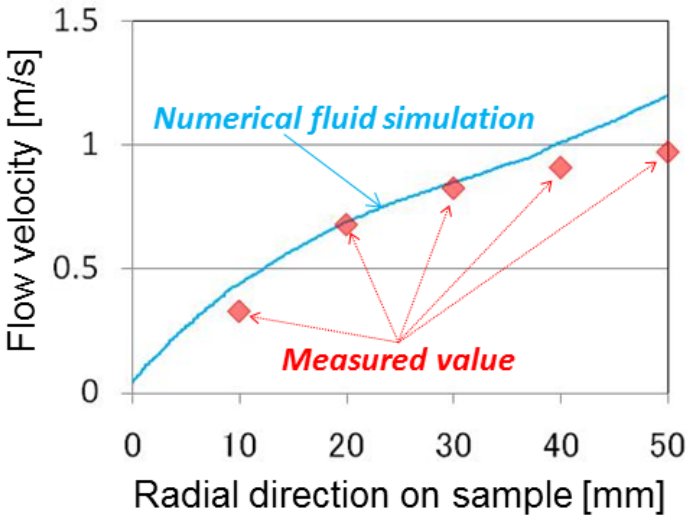


Figure 3.6 Radial direction on sample by the laser sensing fluid visualization measuring device [70].

The experimental result used RD system made of alumina shows several problems by coefficient of thermal expansion between type 316SS coated alumina and unknown oxidation reaction (this reaction were later confirmed according to Li–O reactant in liquid Pb–Li (Chapter 4)). On the other hand, the RD system made of molybdenum also showed no corrosion during this experiment (Figure 3.7).

The chemical composition of Cr, Ni and Mn measured on the reference SUS316 sample as the function of the radial position is shown Figure 3.8. Cr steadily decreased from point 8 (relative velocity, 23 cm/s at 500℃), but Ni steeply decreased from point 6 (relative velocity, about 18 cm/s at 500℃) to point 8. The content of these elements then stayed constant up to the velocity corresponding to about 31.4 cm/s at 500℃. Mn was not detected outside of point 8. In a preliminary test of SUS316, it was possible to observe the effect of change of velocity in the rotating disk system. We also saw that the quantity of corrosion product is large outside the disk, depending on the relative flow velocity, and obtained the result that Cr and Ni corrode selectively (Ni > Cr > Mn).

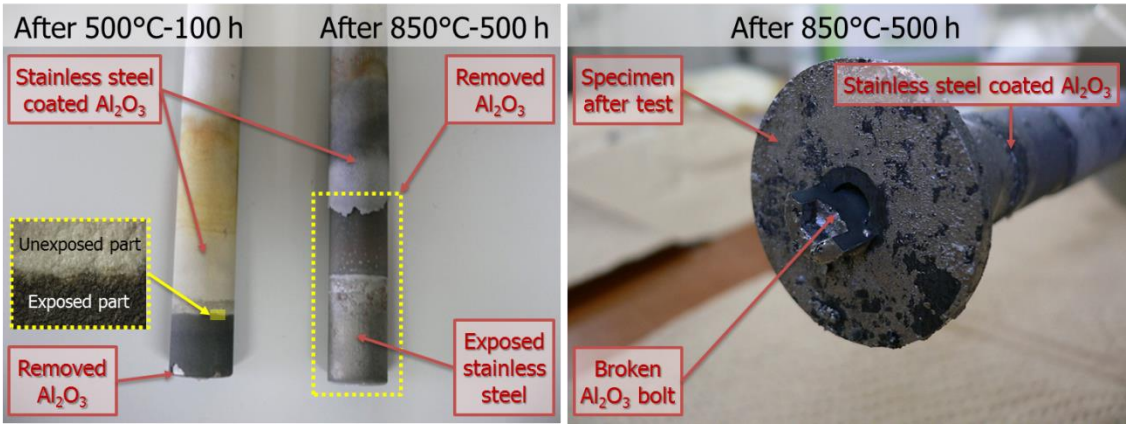


Figure 3.7 Several problems in RD system made of alumina.

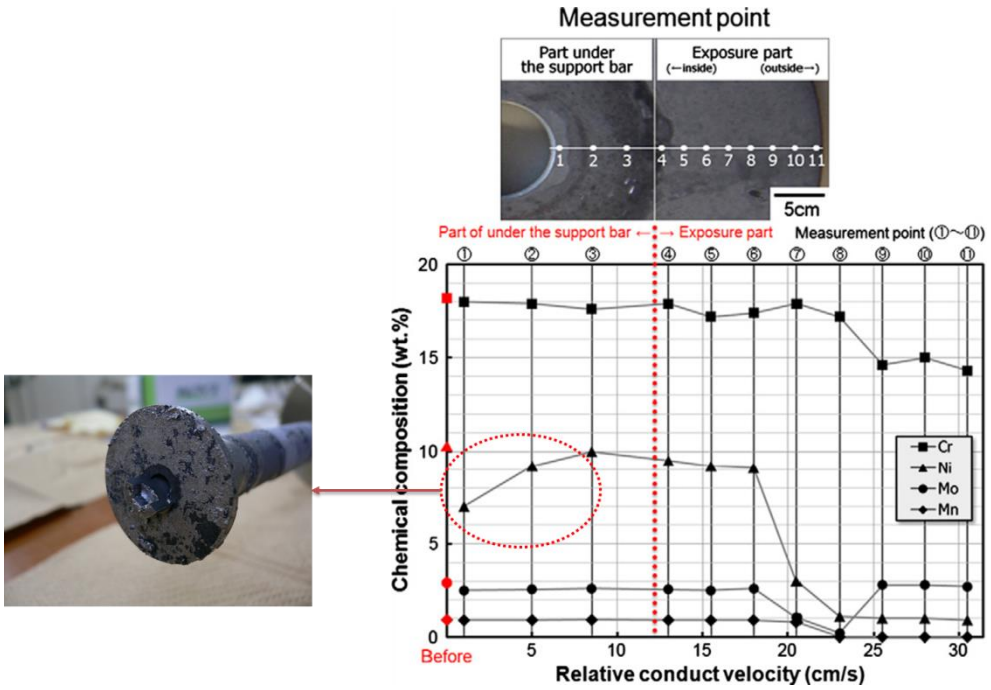


Figure 3.8 Change of chemical composition on SUS316 surface before test and after corrosion test at 500℃ for 500 h.

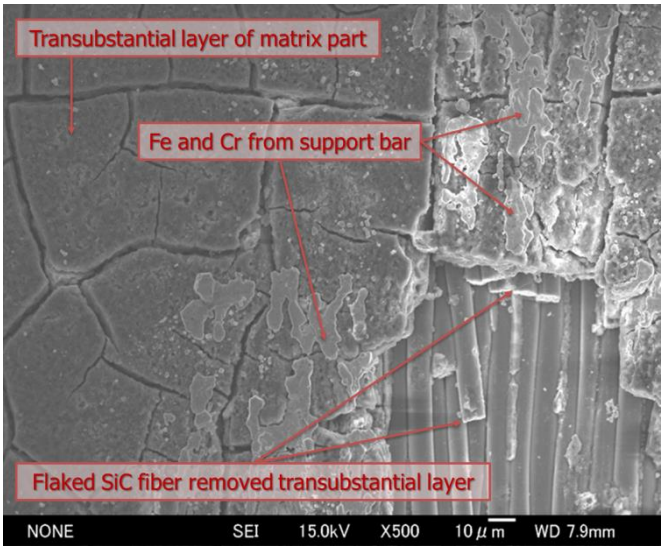


Figure 3.9 Photomicrographs of the surface on NITE–SiC/SiC composite after exposure to liquid metal Pb–Li at 850℃ after 1000 h.

### 3.5.2. NITE–SiC/SiC composite in RD system made of molybdenum

Figure 3.10 shows photomicrographs of NITE–SiC/SiC composite before test and after the corrosion test at 900℃ for 1000 h. The boundary of the matrix and fiber on the surface of the exposed specimen was not clearly distinguished, because the surface adhered layer was not removed. This adhered layer had many cracks (Figure 3.10(b), (c) and (h)). When viewed in cross section, the thickness change of oxidation layer was observed as a function of contact velocity on the surface of the sample. Average thickness at the point with relative velocity 15.7 cm/s (inside) was 27.5 μm and at the point with 34 cm/s (outside) was 45.9 μm. Si, Al and O were detected by EDX analysis in the surface layer after the test at 900℃ for 1000 h (Figure 3.11). On the other hand, this layer did not exist under the support bar unexposed to the liquid Pb–Li. This cracking is believed to be due to differences in thermal expansion between the SiC/SiC composite and the adherent surface oxidation layer during cooling from the 900℃ test temperature to room temperature. In contrast, the sample surface under the support bar did not show such any cracking, since there was no surface oxidation layer. In addition, in the cross section (Figure 3.10(f) and (g)), a proportional correlation is shown between the thickness of the oxidation layer and the relative velocity of the rotating specimen.

On cracked oxidation layer exposed in liquid Pb–Li, we can see the oxidation layer (oxidation of Si, C and Al) under the immersed surface. The density of this oxidation layer seems low. In the case where the SiC fiber was exposed to liquid Pb–Li, on the other hand, we can see that an oxidation layer was formed and grew by the oxidation reaction of Si, C and Al from SiC fibers

exposed to liquid Pb–Li. The fact that Al directly under the oxidation layer is decreased shows that the movement of Al or the oxide may be related to the mechanism of layer formation. $Al_2O_3$ is a component of the sintering additive that is used for forming NITE–SiC/SiC composites and exists mainly in the matrix. Oxygen in the atmosphere is extremely low. Because of this, the source of the oxygen in the adhered layer is unknown. In other research by the authors, even when liquid metal Pb–Li comes in contact with the atmosphere or with gases in a bubble, the oxygen potential of the liquid Pb–Li hardly changes [72]. One possible explanation of the material change, it is that the oxygen source is oxide compounds in Pb–Li formed from elements of the NITE–SiC composites.

For example, it is known that $Li_2O$ reacts to form compounds such as $LiAlO_2$, $Li_2SiO_3$, $Li_4SiO_4$ and etc. [73]. If the oxide exists in compounds in the liquid Pb–Li, chemical changes of SiC composite may have occurred without an oxidation process. Actually, these compounds are easily generated only during high temperature mixing of alumina (or silica) with $Li_2O$. Therefore, excess lithium in liquid Pb–Li may have an effect on the change of compound such as $Al_2O_3$ and $SiO_2$. This chemical change on the SiC composites was observed in microstructures after about 1000 h.

Furthermore, in order to clarify the formation mechanism of the transubstantial layer on the surface of NITE–SiC/SiC composites, the research which used monolithic CVD–SiC material without sintering additives is required.

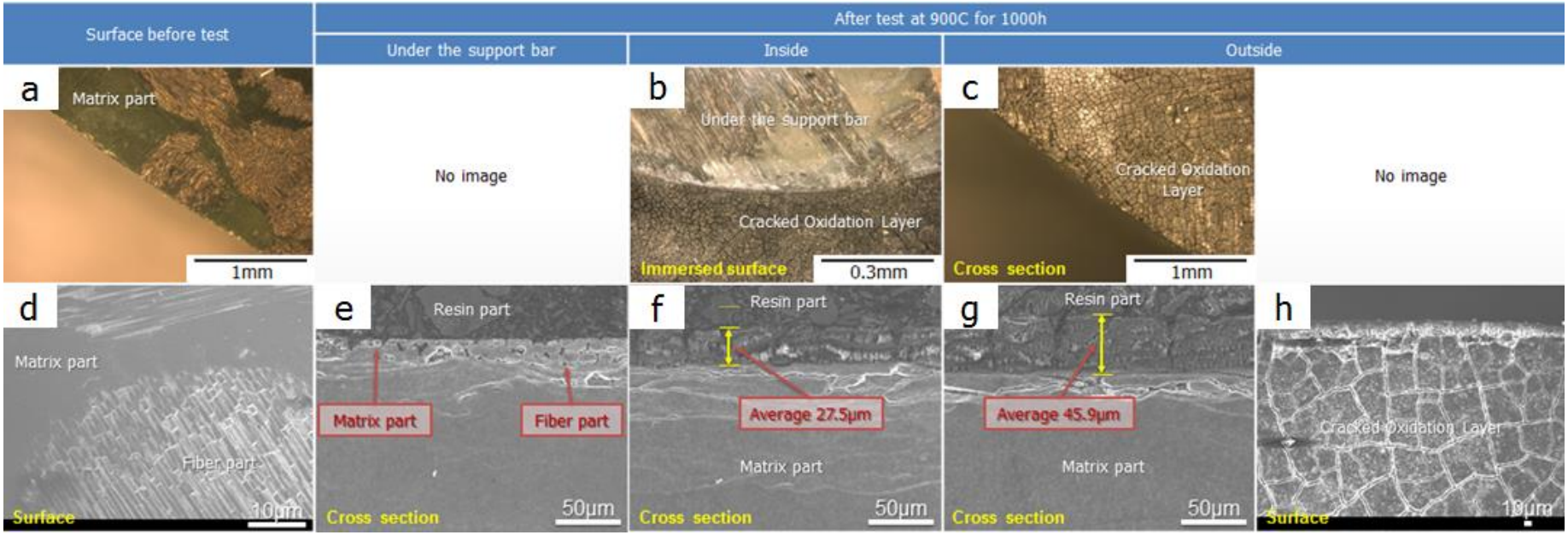


Figure 3.10 Photomicrographs of NITE–SiC/SiC composite before and after the corrosion test at 900℃ for 1000 h.

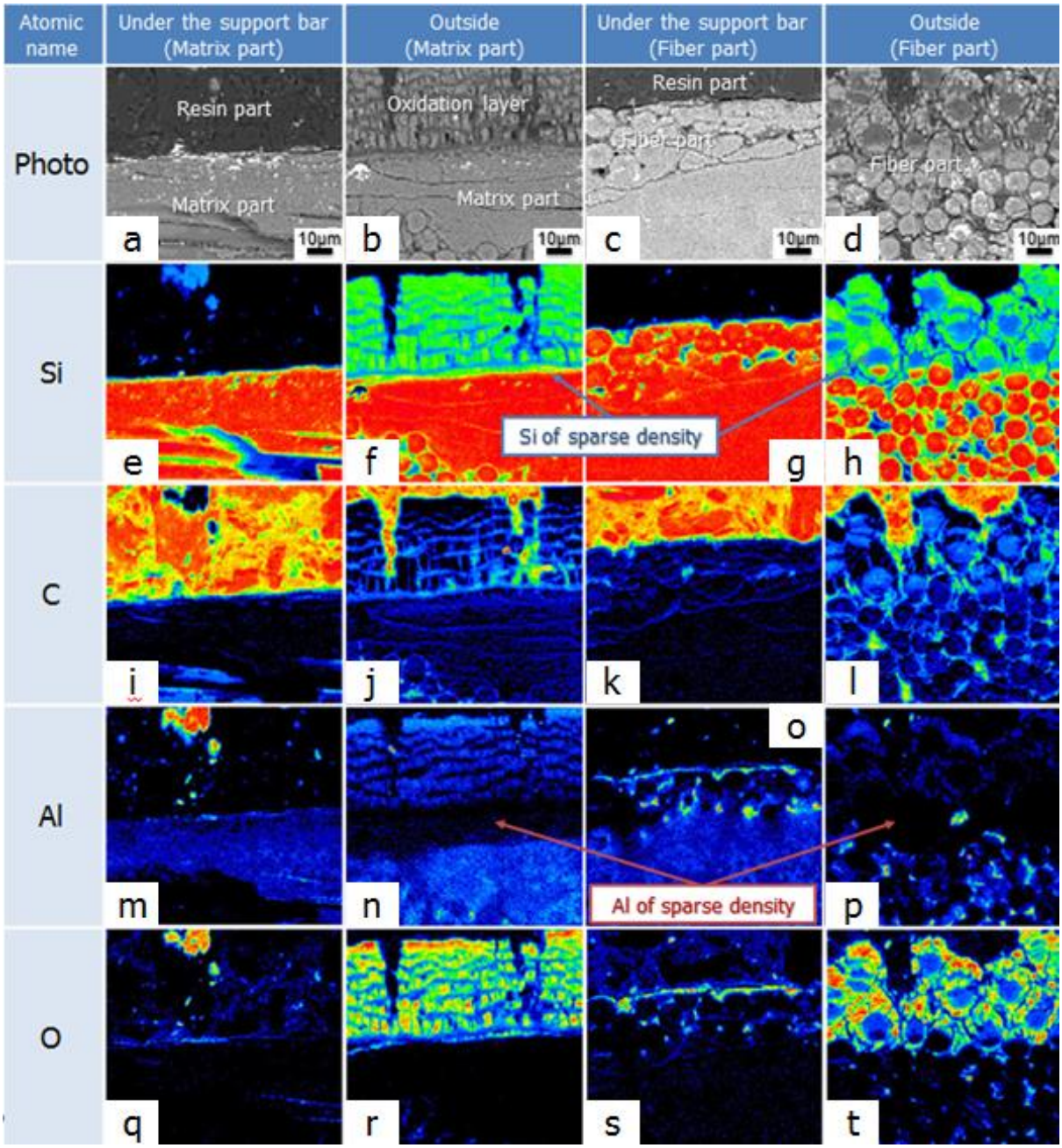


Figure 3.11 EPMA evaluation of the cross-section on NITE–SiC/SiC composite after exposure to liquid metal Pb–Li at 900℃ after 1000 h.

## 3.6. Short summary of chapter 3

In this chapter, two types of simple assembles, rotating disk (RD) systems, were developed and estimated to measure the compatibility of advanced materials exposed to liquid metal Pb–Li with flowing at high temperature. The obtained main results are summarized as follows:

1) It was found that experiment by using RD system made of alumina has a significant reaction with liquid metal Pb–Li at high temperature. This reaction phenomenon was discussed in chapter 4.

2) The rotating disk system made of molybdenum shows soundness and applicability with flowing at high temperature. And on the surface of SUS316 and NITE–SiC/SiC composites using the rotating disk system as preliminary experiment, the surface chemical composition was changed as a function of the radial position.

3) In the experiment in flowing liquid Pb–Li at high temperature, control of oxygen and moisture is important. Especially, in the result of NITE–SiC/SiC composites after the test at 900℃ for 1000 h, the transubstantial layer with crack was found on matrix and fiber on the surface. This layer contained elements of Si, C, Al and O. This phenomenon is assumed to be due to influence by the small amount of sintering additive ($Y_2O_3$, $Al_2O_3$), and discussed in chapter 4, concretely.

# 4. Microstructure and corrosion behavior of SiC materials exposed to liquid metal Pb–Li flowing at 900℃

## 4.1. Introduction

Silicon carbide (SiC) and SiC/SiC composites have become widely used as promising candidate for structural and functional materials of advanced nuclear systems due to their excellent mechanical and thermal properties at high temperatures, low induced activity in the case of high purity and resistance for irradiation, high chemical stability and high heat resistance. Liquid metals lead–lithium (Pb–17Li) are used as a coolant and a tritium breeder for the blanket systems of fusion reactors. SiC and SiC/SiC composites is considered as most structural and/or functional applications in contact with these liquid materials. SiC ceramics are integrated as critical components in a system, which has to be frequently contacted to selected breeder/coolant provide attractive options for high tritium breeding ratio, high efficiency and simplicity of high temperature blanket system [25].

As described in Section 2.1, Chapter 2, one of the critical issues for the biomass-fusion hybrid concept is the compatibility evaluation of SiC and SiC/SiC composites with liquid metal Pb–Li. The compatibility of materials with Pb–Li has been studied on several advanced materials by static condition or flowing condition with complicated convection system. In those studies, however, investigation on mechanism and micro-chemical processes of the SiC materials in the liquid metals Pb–17Li with flowing at high temperature are quite limited. Any data are not available for SiC and SiC/SiC composites among the advanced materials yet. In the present work using a simple RD system for high temperature with flowing condition, corrosion behavior of monolithic CVD SiC and NITE–SiC/SiC composites have been investigated and compared in liquid metal Pb–17Li up to 1000 h at 900℃ to clarify the effects of sintering additives ($SiO_2$, $Al_2O_3$ and $Y_2O_3$) and flowing contact velocity, etc.. The formation mechanism of the transubstantial layer on monolithic CVD SiC and NITE–SiC/SiC composites in high temperature with flowing will be proposed based on the analysis of the oxide scales formed on the specimen surface.

## 4.2. Experimental procedure

### 4.2.1. Experimental conditions

In the previous chapter, the schematic of the compatibility analysis system (RD system made of Mo) are shown in Figure 3.4 in section 3.3, Chapter 3. It has been demonstrated that RD system has the feasibility of compatibility test with flowing condition at high temperature.

The compatibility analysis was improved and performed by the RD system with flowing condition. This RD system to rotate two disk samples in a liquid metal was used to measure the effect of flow speed as a function of the radial position on the disk (diameter: 30 mm → 50 mm). This system, consisting of the electric furnace, the crucible with panels, the support bar with guide, thermocouple and electric motor, was placed under a high purity argon gas atmosphere in a glove box, where humidity and oxygen impurity were continuously kept less than 0.01 ppm. Two disk samples were mounted on the support rod and were immersed in the crucible containing liquid metal. The disks were rotated and exposed to the flow with various relative speeds. The crucible contained about 1.5 kg of Pb–Li and was heated to the temperature range (~ 900℃) by the electric furnace. The temperature was measured and controlled with type K thermocouples contained in a central molybdenum tube. All materials for the crucible, support rod, thermocouple protection tube, etc. that contacted liquid Pb–Li were molybdenum which was expected and reported to be compatible with lithium–lead alloy [61, 62, 69]. This apparatus also showed no corrosion during this experiment.

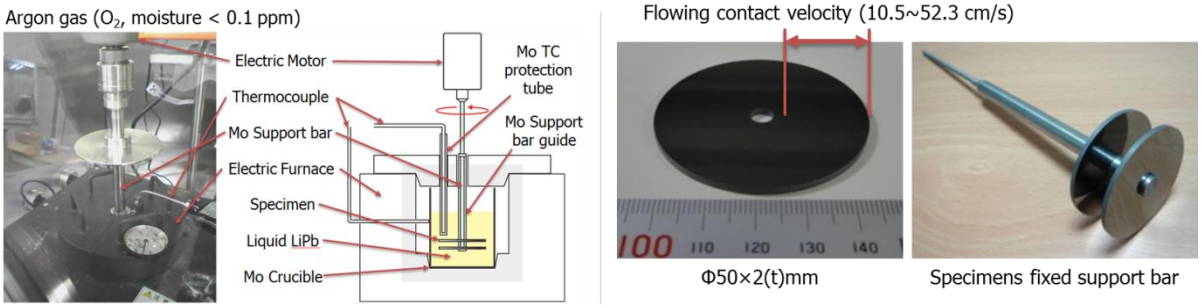


Figure 4.1 Schematic compatibility test assemble by improved RD system.

### 4.2.2. Sample and operating condition

Table 4.1 presents the operating conditions of corrosion tests by RD system. The rotation speed of the support rod was about 200 rpm. The equivalent flow velocity is a function of radial position on the disk and ranged ~10.5 to 52.3 cm/s.

Table 4.1 Opterating conditions of corrosion tests by RD system.

| Material | Temperature (℃) | Duration (h) | Diameter (mm) | Relative flow velocity (cm/s) |
|---|---|---|---|---|
| NITE–SiC/SiC composites | 900 | 100 | 50 | 10.5–52.3 |
| | | 300 | 50 | 10.5–52.3 |
| | | 500 | 50 | 10.5–52.3 |
| | | 1000 | 50 | 10.5–52.3 |
| Monolithic CVD SiC | 900 | 500 | 50 | 10.5–52.3 |
| | | 1000 | 50 | 10.5–52.3 |

The specimens used for the corrosion tests were SiC/SiC composites produced by the NITE process [22, 60]. The composite contains the SiC fiber (Tyranno-SA 3rd, Ube Ind.) coated with C (thickness of the carbon interface was 200–300 nm). Density of the NITE–SiC/SiC was 3.01 g/cm$^3$. The shape of the specimen was a circular plate. The size of the specimen used was 50 mm diameter and 2 mm thickness. The size of the samples used these corrosion test was larger than that used corrosion test in chapter 3. In order to eliminate the superficial oxide layer, the surfaces of specimen were finely polished using diamond powder of 0.25 μm in a diameter before the tests. Then, the specimens were cleaned in an alcohol–acetone mixture. The specimens tested in the Pb–Li were taken out from the liquid Pb–Li after the test. Then, the specimens were mainly cleaned with an acetic acid–hydrogen peroxide–ethanol mixture (1/3:1/3:1/3) at RT (25℃) until the specimen weight reached a constant value by the removal of adhered Pb–Li from the specimen surface [69]. After the rinse of the specimens in the ethanol, the cleaning of the specimen was finished in an acetone.

The morphologies of surface and cross section were characterized by optical microscopy, scanning electron microscopy (SEM) and energy dispersive spectroscopy (EDS). Composition profiles for the major elements before and after the compatibility tests were measured by field emission scanning electron microscope (FE-SEM) installed in field emission electron probe micro analyzer (FE-EPMA, JXA-8500FK, JEOL co., Japan). The phase constitution of the as-deposited coatings was examined by X-ray diffraction (XRD), using Cu Kα radiation.

Further, for the lithium element analysis, depth profiles of surface after the compatibility tests were measured by GD-OES (Glow discharge optical emission spectrometry, HORIBA co., Japan, Figure 4.2). And composition profiles for bonding state of the elements including the Li element after the compatibility tests were measured by SXES (Soft X-ray emission spectroscopy, JEOL co., Japan, Figure 4.3). The SXES gives information of electronic structure of

bonding electrons, and combined with microscopy should be a hopeful method to reveal physical properties and chemical bonding states of identified small specimen areas of various compounds.

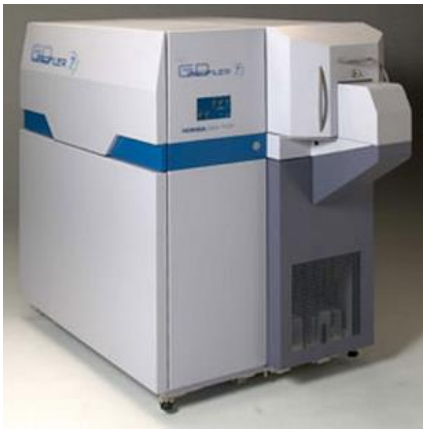

Figure 4.2 GD-OES (Glow discharge optical emission spectrometry, HORIBA co., Japan)

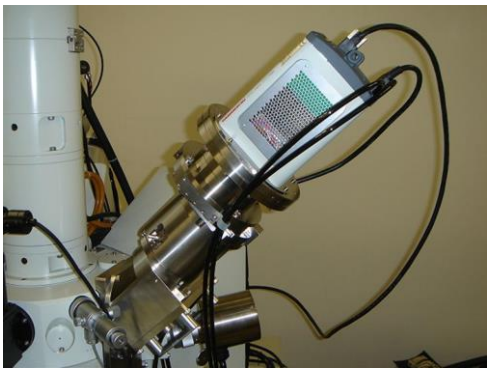

Figure 4.3 SXES (Soft X-ray emission spectroscopy, JEOL co., Japan)

## 4.3. Results and discussions

### 4.3.1. Compatibility analysis on monolithic CVD–SiC

#### 4.3.1.1. Morphology on monolithic CVD–SiC

Cross-section morphology of monolithic CVD–SiC exposed at 900℃ for 1000 h are given in Figure 4.4. The microstructure was quite different from that of the specimen exposed to the static Pb–17Li. Monolithic CVD–SiC material in static pot was considered as good for compatibility to liquid metal Pb–Li [35], but not necessarily at a high temperature region of 900℃ level as shown Figure 4.4(c). The thickness change of the transubstantial layer was observed as a function of contact

velocity on the surface of monolithic CVD–SiC. Average thickness at the point with relative velocity 50.2 cm/s (outside) was average 11.9 μm (Figure 4.4(a)). On the other hand, this layer did not exist inside disk (> 15 mm) as shown Figure 4.4(a) and (b). Si, O and Pb were detected by EDX analysis in this layer. Also, the density of C is higher than a matrix part. It is proper to regard C detected in EDX as abrasives of diamond buried in the transubstantial layer.

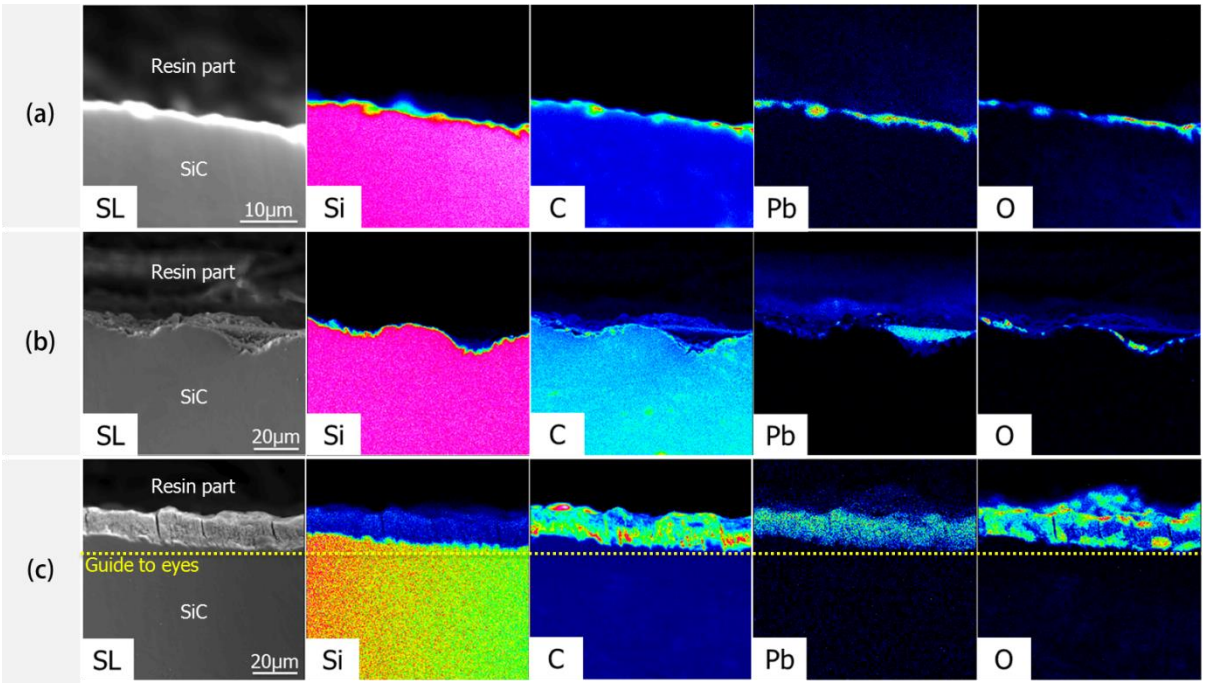


Figure 4.4 EPMA evaluation of monolithic CVD–SiC after exposure to liquid metal Pb–Li at 900℃ after 1000 h: (a) under the support bar unexposed to liquid Pb–Li, (b) 10 mm away the center (about 31.4 cm/s), (c) 24 mm away from the center (about 50.2 cm/s).

Figure 4.5 shows depth profile by the GD-OES of monolithic CVD–SiC after exposure to liquid metal Pb–Li at 900℃ after 1000 h. The under part of Pb adhesion on the surface of monolithic CVD–SiC is considered for the concentration of Li, O and Si to be high (Li > O > Pb), and to correspond with formation of the Li–Si oxidation.

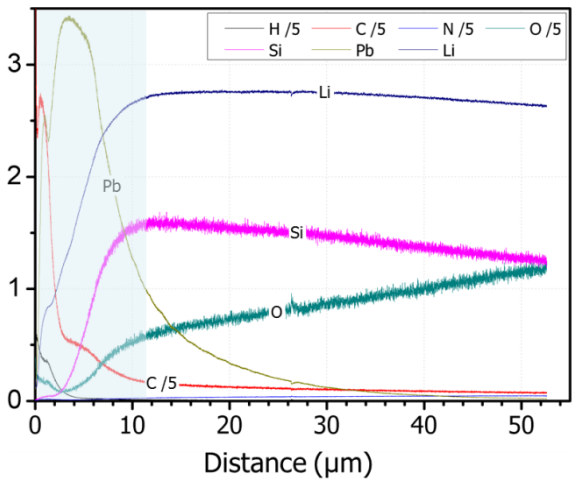


Figure 4.5 Depth profile by GD-OES of monolithic CVD–SiC after exposure to liquid metal Pb–Li at 900℃ after 1000 h (Electrode pulse: 25%, diameter: 4 mm).

Figure 4.6 shows the SXES evaluation of monolithic CVD–SiC after exposure to liquid metal Pb–Li at 900℃ after 1000 h. Satellite peaks of Si–O, which is considered from the comparison with the peak value of the substrate of SiC, and corresponds to the formation of Si oxidation (such as $SiO_2$) in the transubstantial layer was observed. When compare the results of O-K (consistent with Li) and Pb-N (contradictory with Li), a satellite peak of Li which is supposed to correspond the formation of Li oxide was observed. Therefore, XRD pattern of monolithic CVD–SiC after 1000 h detected the $Li_4SiO_4$ in the transubstantial layer such as Figure 4.7.

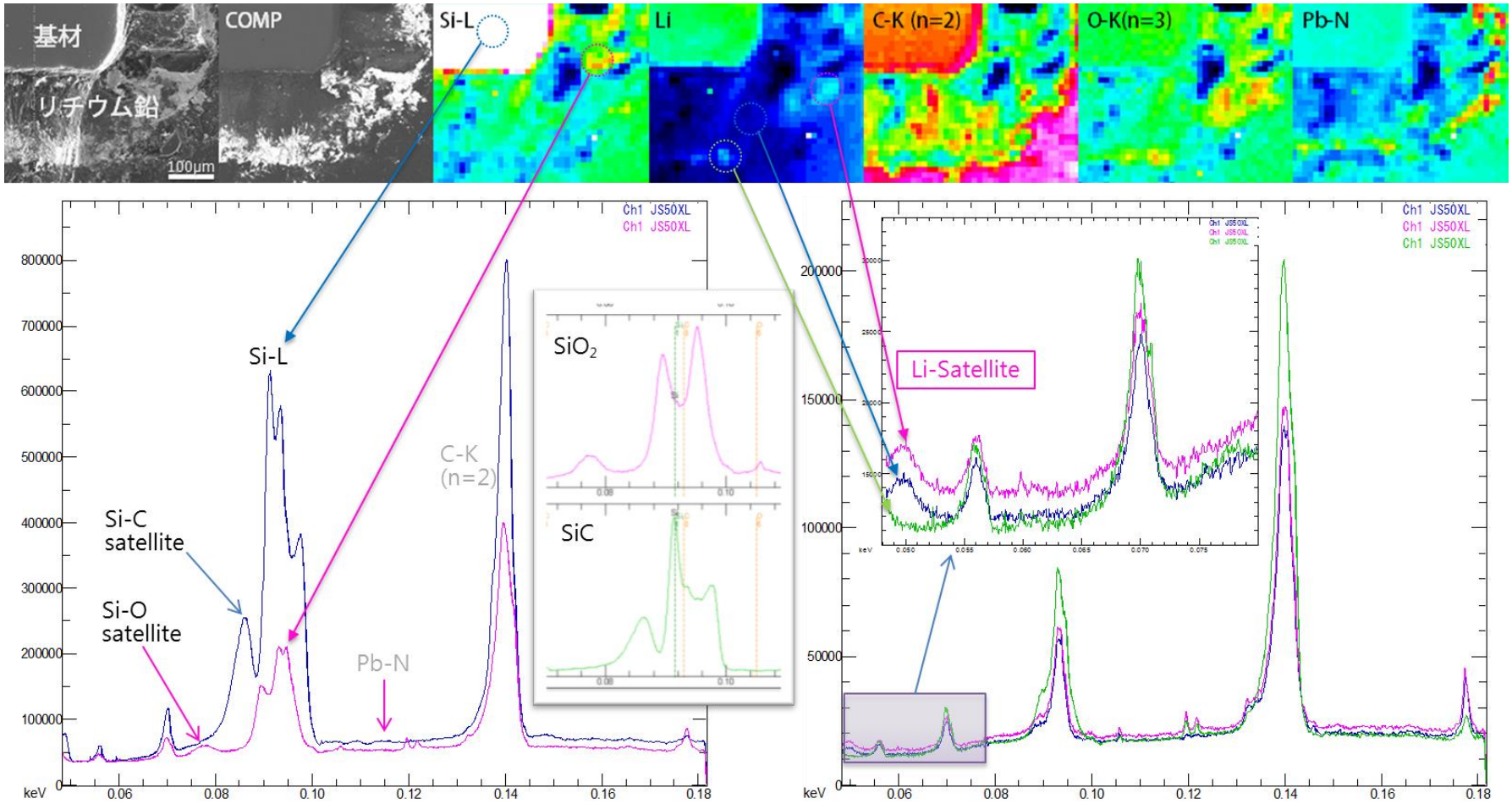


Figure 4.6 SXES evaluation of monolithic CVD–SiC after exposure to liquid metal Pb–Li at 900℃ after 1000 h.

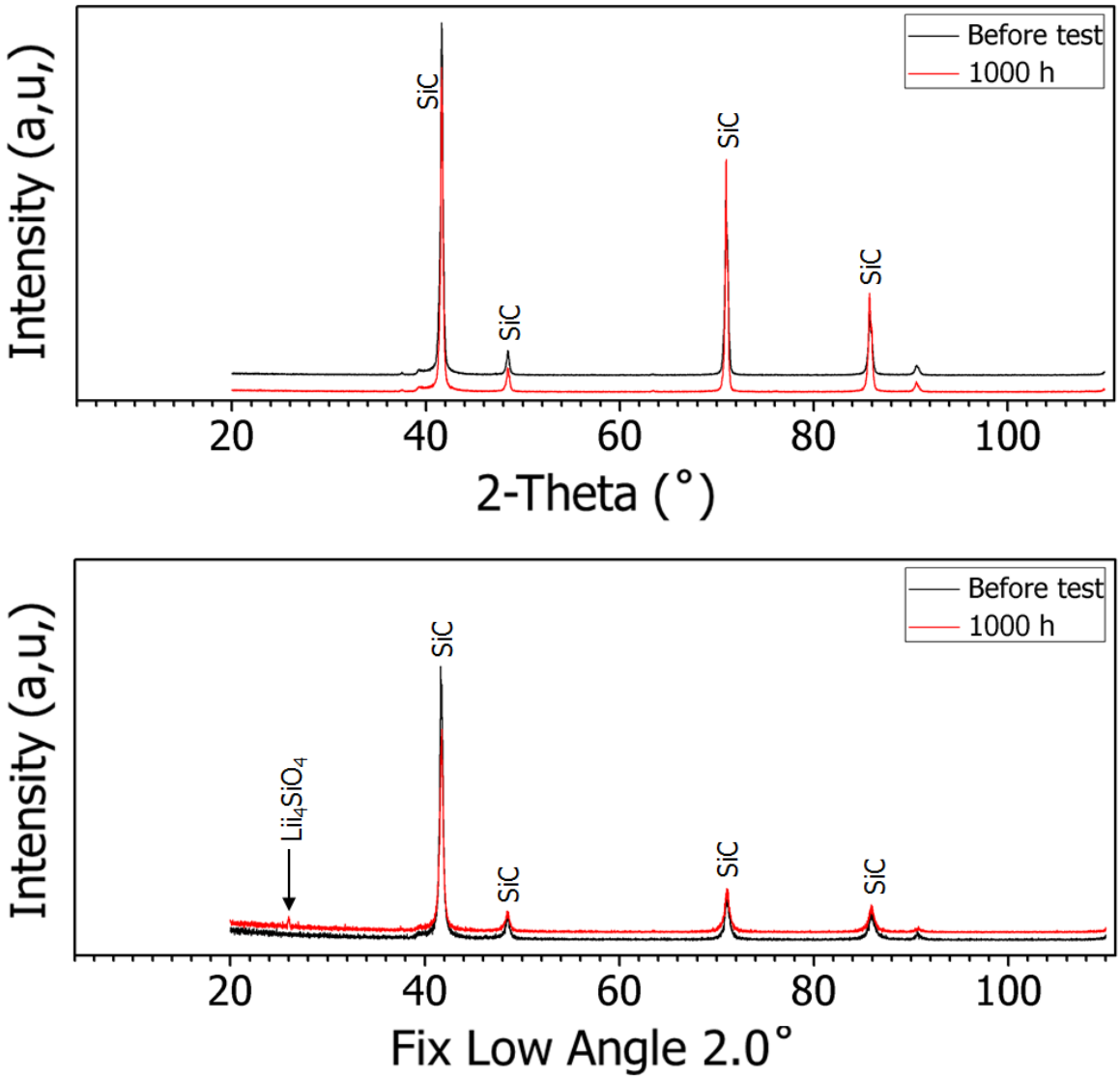


Figure 4.7 XRD result of the transubstantial layer on the surface of monolithic CVD–SiC exposed at 900℃ after 1000 h.

### 4.3.2. Compatibility analysis on NITE–SiC/SiC composites

#### 4.3.2.1. Surface morphology on NITE–SiC/SiC composites

Figure 4.8 shows SEM surface image of NITE–SiC/SiC composite specimens before and after the compatibility tests in Pb–Li at 900℃. In case of the tests up to 500 h, the boundary of the matrix and fiber on the surface of the exposed specimen was not clearly distinguished, because the surface adhered layer was not removed. This adhered layer had many cracks. When viewed in cross section, the thickness change of layer was observed as a function of contact velocity on the surface of

the sample. On the other hand, this layer did not exist under the support bar unexposed to the liquid Pb–Li.

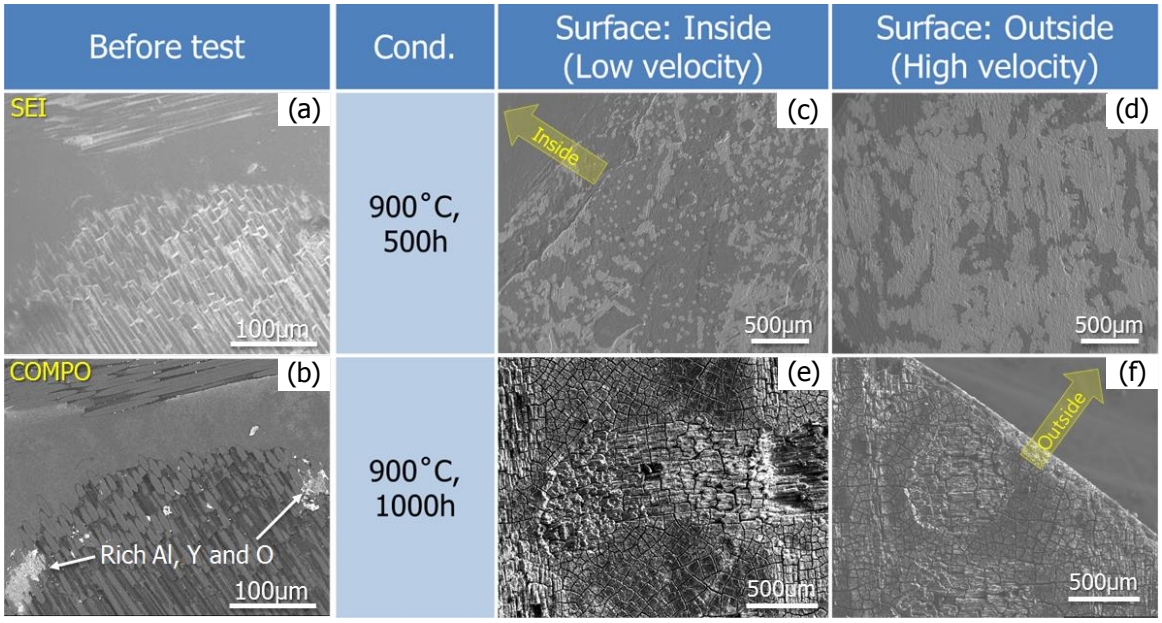


Figure 4.8 Surface morphologies on the NITE–SiC/SiC composites before and after exposure to liquid Pb–Li at 900℃: change by a disk radial direction.

### 4.3.2.2. Cross-section morphology on NITE–SiC/SiC composites

Figure 4.9 and Figure 4.10 show the SEM cross-sectional image of the tested specimen and the EDS analysis results up to 1000 h at 900℃. After exposures, height change of each specimen was confirmed by diameter. The thickness change of this layer steadily increased from 5 mm diameter (relative velocity, 10.47 cm/s) to 25 mm (relative velocity, 52.36 cm/s) of specimen. In case of 1000 h, it was higher than that of 500 h. We also saw that the quantity of corrosion layer is large outside the disk, depending on the relative flow velocity, and obtained the result that layer of Y corrode selectively (Figure 4.9). At the interface between the adhered Pb–Li and the substrate, Y rich layer and was detected, and the layer must be the Li–O–Y layer. Therefore, this layer did not observed on the specimen after 1000 h test. In the result after 500 h, the element analysis of the oxide layer contains Al, Y, O as well as Si and C (the main ceramic components). On the other hand, specimen surface after exposure for 1000 h had shown no detectable Y element. Especially, The Y content in the oxide layer was higher than that in the main matrix (in cross-section after 500 h). In the result after the test for

1000 h, an oxide layer was found on matrix and fiber near the surface. This layer contained Si, Al and C, and also seems to have a low density.

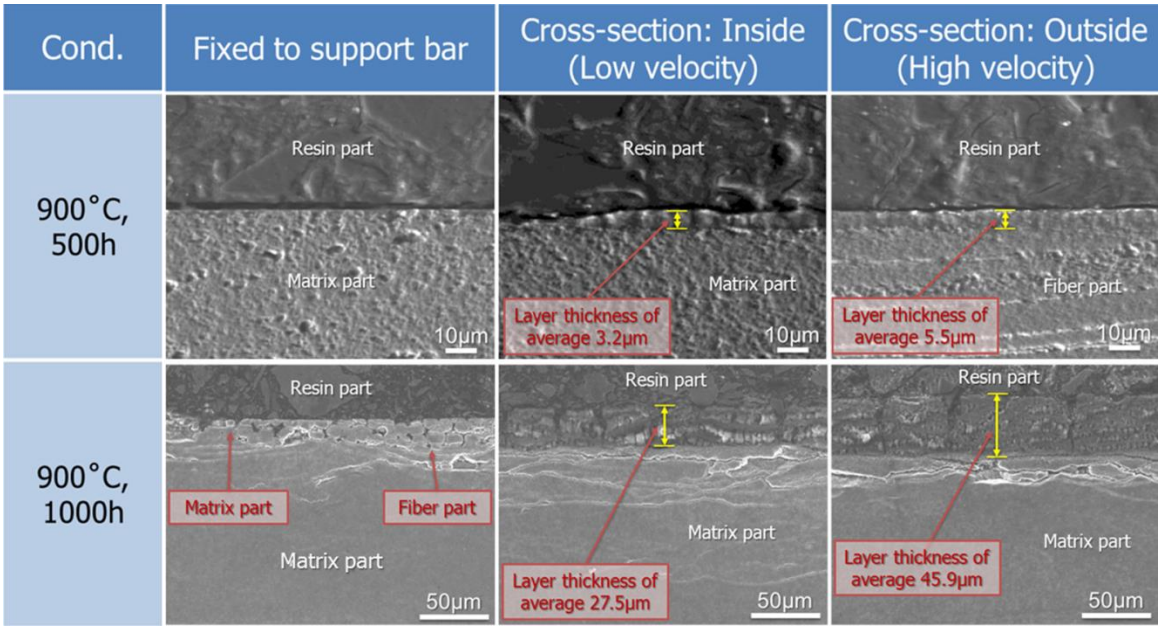


Figure 4.9 Cross-section morphologies of NITE–SiC/SiC composites after exposure to liquid metal Pb–Li at 900℃: change by a disk radial direction.

The dissolution of a Li–Y–O layer formed on the specimen surface after 500 h exposure was accelerated after 1000 h exposure. That there were a lot of crack layer on the specimen surface after the immersion to the Pb–Li for 500–1000 h. The specimen surface after 500 h test revealed the preferential layer of Y on the crack layer as the layer, which was observed after 1000 h exposure. Figure presents that the Y on the specimen surface was slightly depleted by 500 h exposure of NITE–SiC/SiC composites. This indicated the depletion of the Y from the SiC/SiC composites into the Pb–Li was rapid more than that of Al in the short duration within 1000 h. XRD pattern of sample after 500 h shows the layer contained Y element was confirmed $Y_2O_3$ and $Li_4SiO_4$. (Figure 4.11). On the other hand, we can't see $Y_2O_3$ and $Li_4SiO_4$ in test after 1000 h. As duration goes by, the oxide layer was found the $SiO_2$ near the surface. A known oxidation except $SiO_2$ was not identified for 1000 h.

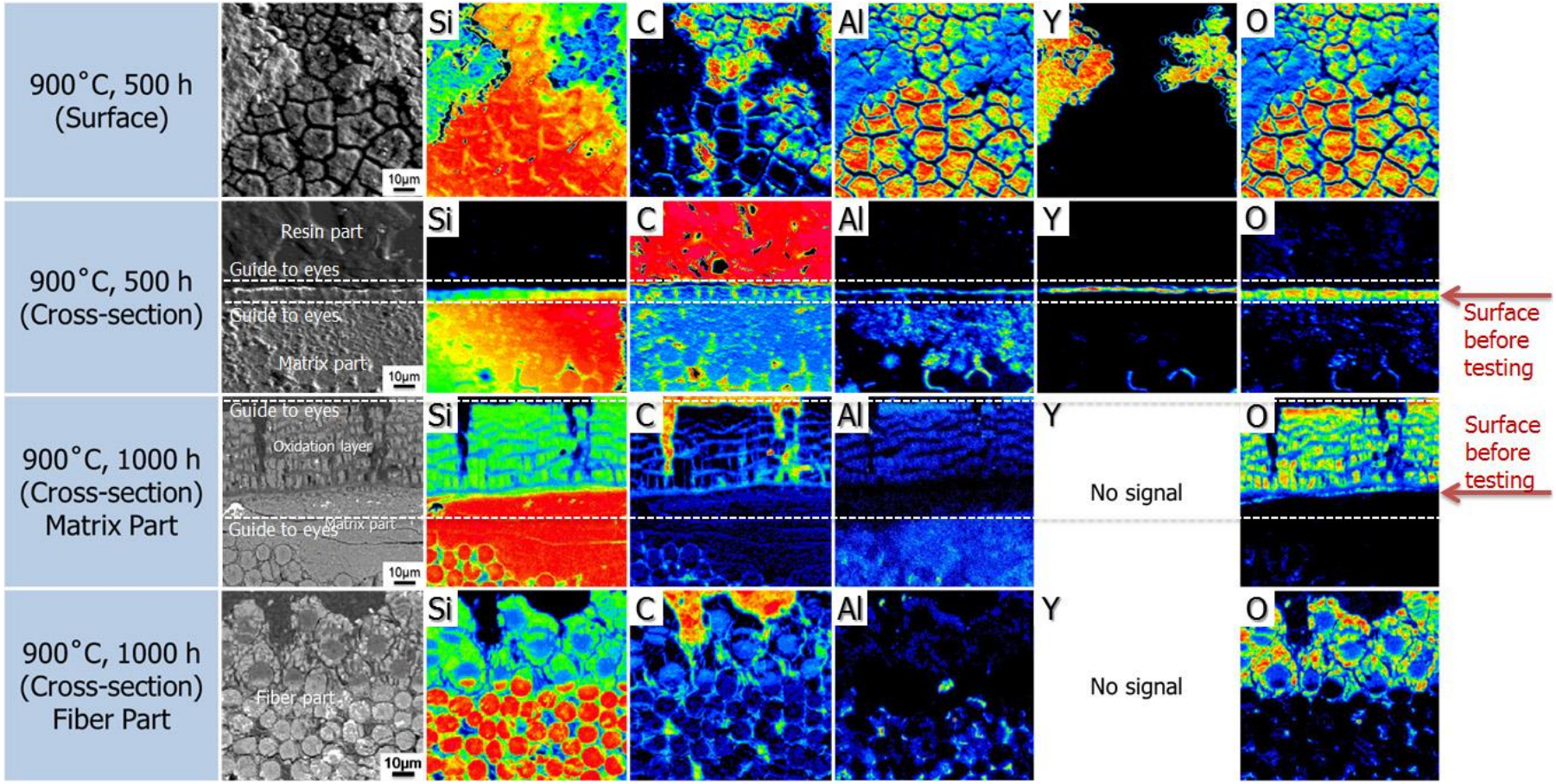


Figure 4.10 EPMA evaluation of NITE–SiC/SiC composites after exposure to liquid metal Pb–Li at 900℃.

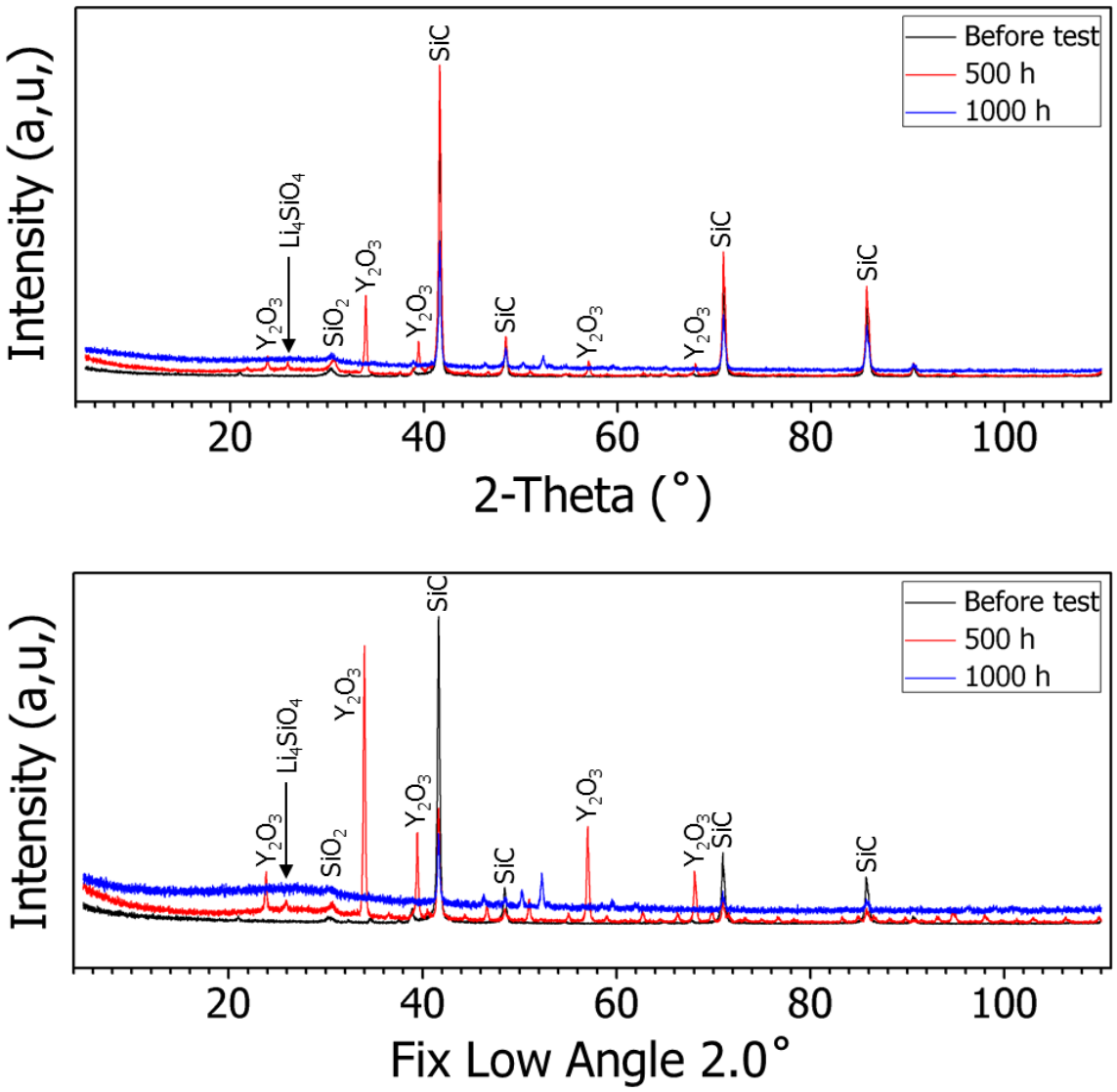


Figure 4.11 XRD result of the transubstantial layer on the surface of NITE–SiC/SiC composites exposed at 900℃.

### 4.3.3. Height change of the transubstantial layer by flow contact velocity

Figure 4.12 shows the cross-section of NITE–SiC/SiC composite for 1000 h at 900℃. After exposures, height change of each specimen was confirmed by diameter. The thickness change of this layer steadily increased from 5 mm diameter (relative velocity, 10.47 cm/s) to 25 mm (relative velocity, 52.36 cm/s) of specimen. In case of test after 1000 h, it was higher than that of test after 500 h. We also saw that the quantity of the transubstantial layer is large outside the disk, depending on the relative flow velocity and duration.

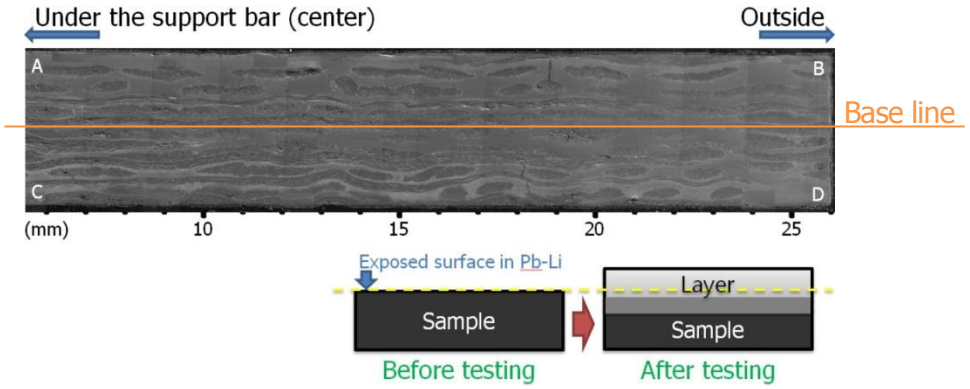


Figure 4.12 Height change of specimen cross-section.

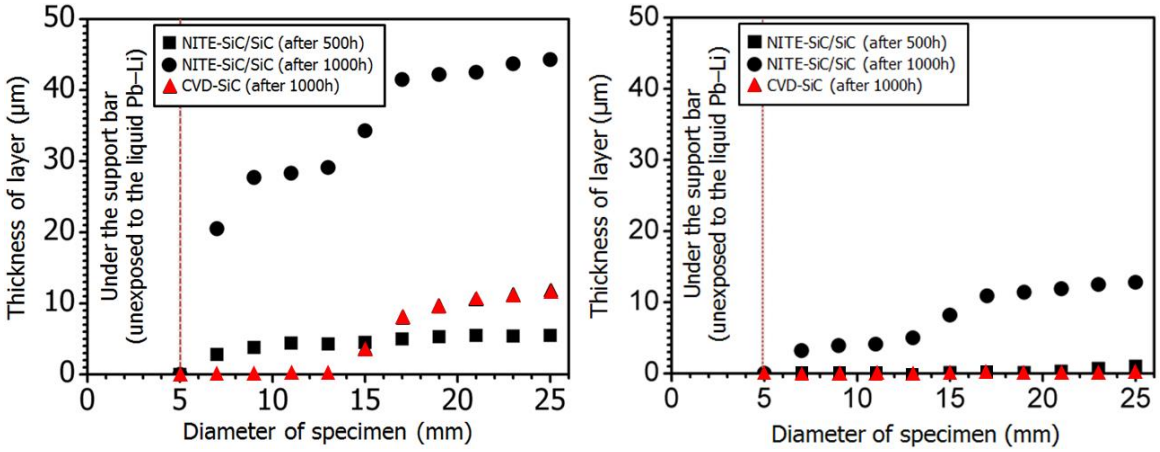


Figure 4.13 Height change of reaction layer on cross-section: (a) Thickness change of the transubstantial layer by disk radial direction, (b) height change of the transubstantial layer by disk radial direction.

### 4.3.4. Measurement of the amount of oxygen in the Pb–Li

The amount of oxygen in the liquid Pb–Li before test was measured by solid electrolytic cell (Figure 4.14). Electromotive force was measured indicating that oxygen potential is low (= theory equilibrium value of oxygen concentration in the liquid Pb–Li) in the liquid Pb–Li before test. The electromotive force measurement of the oxide ionic conductor cell showed oxygen with a pressure of $10^{-47}$ Pa (oxygen pressure close to equilibrium thermodynamics) was presented in the liquid Pb–Li at 500℃ such as Figure 4.15. It was able to confirm that oxygen in the liquid Pb–Li used for this experiment was more likely to exist as Pb–17Li–O, Li–O than Pb–O (Oxygen is incorporated into the liquid Pb–Li, it forms oxidation immediately).

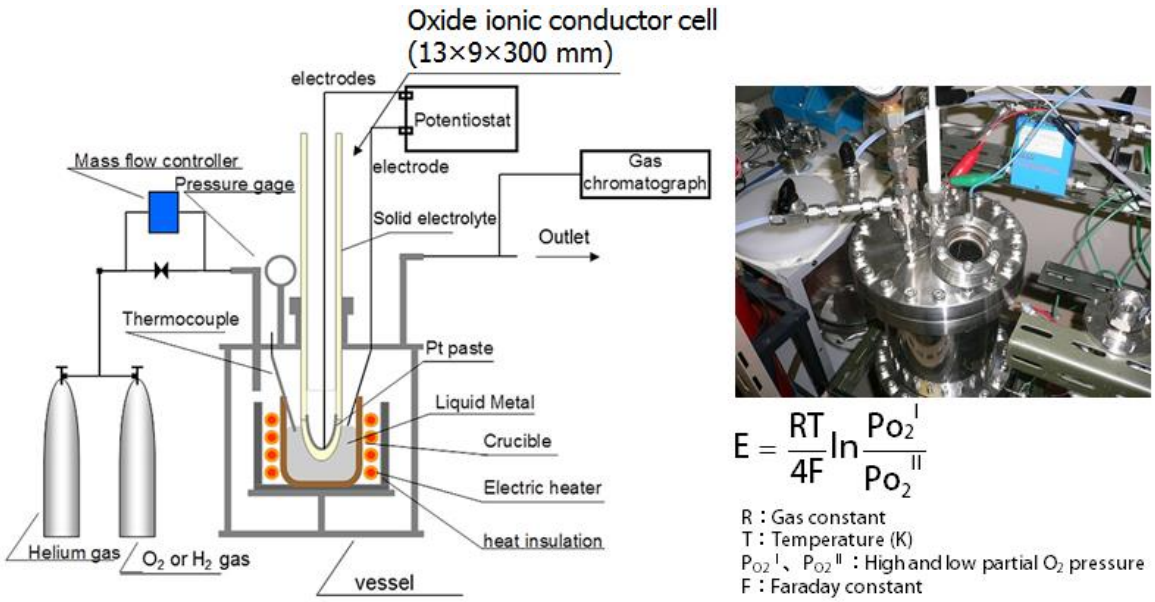


Figure 4.14 the oxide ionic conductor cell for measurement of oxygen concentration in Pb–Li.

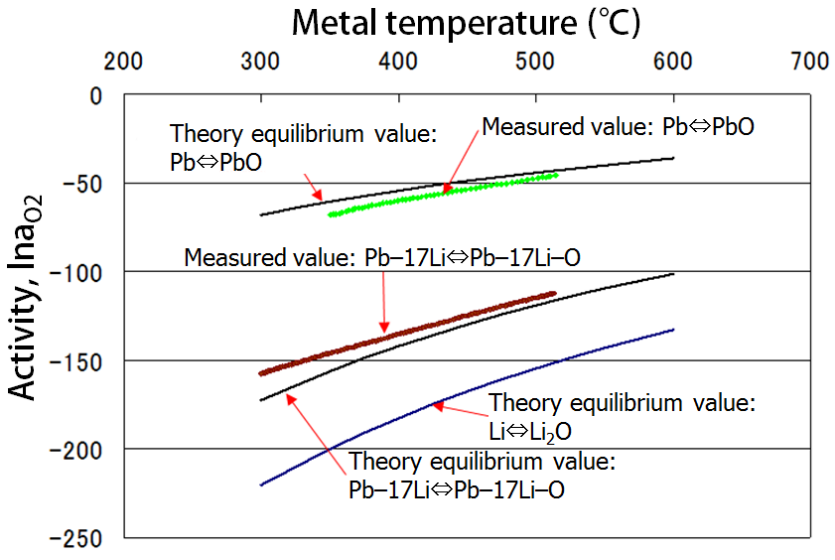


Figure 4.15 Comparison of the measured oxygen activity and balanced oxygen pressure.

### 4.3.5. Discussion and modeling on the transubstantial mechanism of SiC materials

Figure 4.18 shows schematic illustration of chemical reaction mechanism between NITE–SiC/SiC composite and $Li_2O$ in the liquid Pb–Li with flowing condition at 900℃. The reaction products such as Li–O–Si and Li–O–Al might be formed on the surface in the liquid Pb–Li. These

products were not stable on surface of substrate material and dissolved in the Pb–Li. There is no changes experimental results after 300 h, but the transubstantial layer can be confirmed on the surface from 500 h. The depletion of Al and Si on the specimen surface was caused in the liquid Pb–Li from 500 h. These points indicated Y could be easily depleted in the initial stage of the corrosion, though the total corrosion loss was determined by the dissolution of Al at the present isothermal condition. One possible idea for the preferential dissolution of Y is the higher formation energy for $Y_2O_3$ than that for Al oxides. After the oxide is used for the reaction with Y, small quantity of oxide is available for the reaction with Al on ceramic surface. And we can see to cohere on the transubstantial layer from one of $Y_2O_3$ which there is in the grain boundary of the NITE–SiC/SiC composite (Stability: $Y_2O_3$ > $Li_4SiO_4$ > $LiAlO_2$ > $Li_2SiO_3$ > $SiO_2$, Figure 4.16).

In general, the compatibility mechanism of materials can be explained by primary transporters, which are composed of inward diffusing oxygen or outward diffusing metals. This could significantly increase the solubility of many elements in the liquid Pb–Li at high temperature, such as $SiO_2$, $Al_2O_3$ and $Y_2O_3$ by the chemical equations. The possible chemical reactions on the surface of NITE–SiC/SiC composites are:

$$SiO_2 + 2Li_2O_{(in\ Pb–Li)} \rightarrow Li_4SiO_4 \quad (4.1)$$

$$Al_2O_{3(in\ NITE–SiC/SiC)} + Li_2O_{(in\ Pb–Li)} \rightarrow 2LiAlO_2 \quad (4.2)$$

$$SiO_{2(in\ NITE–SiC/SiC)} + Li_2O_{(in\ Pb–Li)} \rightarrow Li_2SiO_3 \quad (4.3)$$

Therefore, it is considered that oxide reactants (such as $Li_2O$) in liquid metal Pb−Li at 900℃, it is considered elements of sintering additives is in the tendency eluted to Pb−Li. These reactions are related to low-density of the transubstantial layer on surface of NITE−SiC/SiC composite. Also, it is regarded that the weakness of $Al_2O_3$ ceramic (in chapter 3) and sintering additives ($SiO_2$, $Al_2O_3$ and $Y_2O_3$) in the NITE–SiC/SiC composites were caused by the reaction of $Li_2O$ in the liquid Pb–Li at 900℃.

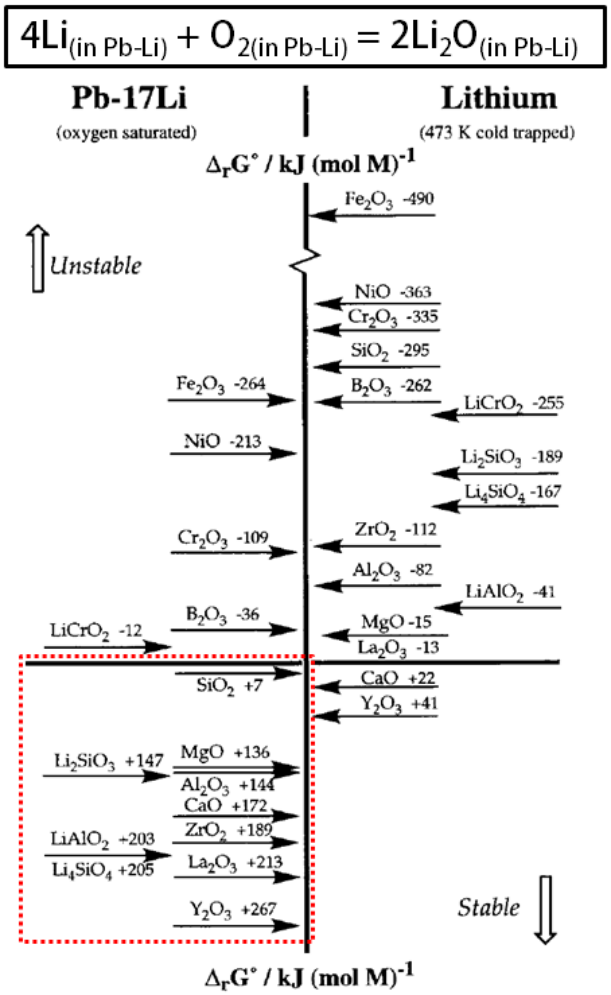


Figure 4.16 $\Delta_rG^0$ (kJ (mol M)$^{-1}$) data for the reaction at 773K of various oxide ceramics with oxygen saturated Pb-17Li and with 473K cold trapped lithium ($x_O$=3.2110$^{-6}$) [74].

Experiment results on monolithic CVD–SiC at 900℃ up to 1000 h by the RD system, it was found to form the transubstantial layer having a thickness of average 11.9 μm in the outer surface regime (relative contact velocity corresponds to about 35-52 cm/s). It is the oxidation containing Si and Li was suggested the transubstantial layer. Oxygen concentration in the glove box of the high purity Ar gas atmosphere is minimal, it is regarded that the transubstantial layer on surface was formed at the reaction of $SiO_2$ which is natural layer and $Li_2O$ in the liquid Pb–Li (refer result of SXES including $SiO_2$). The possible chemical reaction on the surface of monolithic CVD–SiC is:

$$SiO_2 + 2Li_2O_{(in\ Pb\text{–}Li)} \rightarrow Li_4SiO_4 \qquad (4.4)$$

The formation of $Li_4SiO_4$ is suggested that NITE–SiC/SiC composite under same conditions. The transubstantial layer seen thicker on the outside of the disk position, as the supply of

$Li_2O$ is faster (outside of the disk sample), reaction with $SiO_2$ on surface is likely to occur by the flowing of the liquid Pb–Li. However, it is regarded that thickness of the formed the transubstantial layer was not increase from specific thickness.

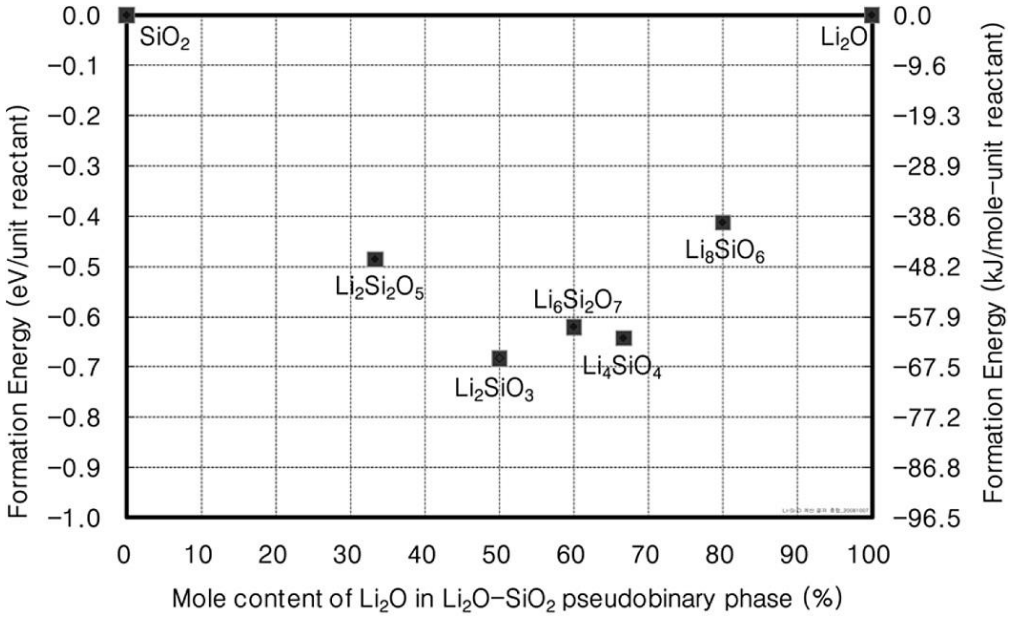


Figure 4.17 The formation energies of stable Li-Si-O phases based on unit reactant [73].

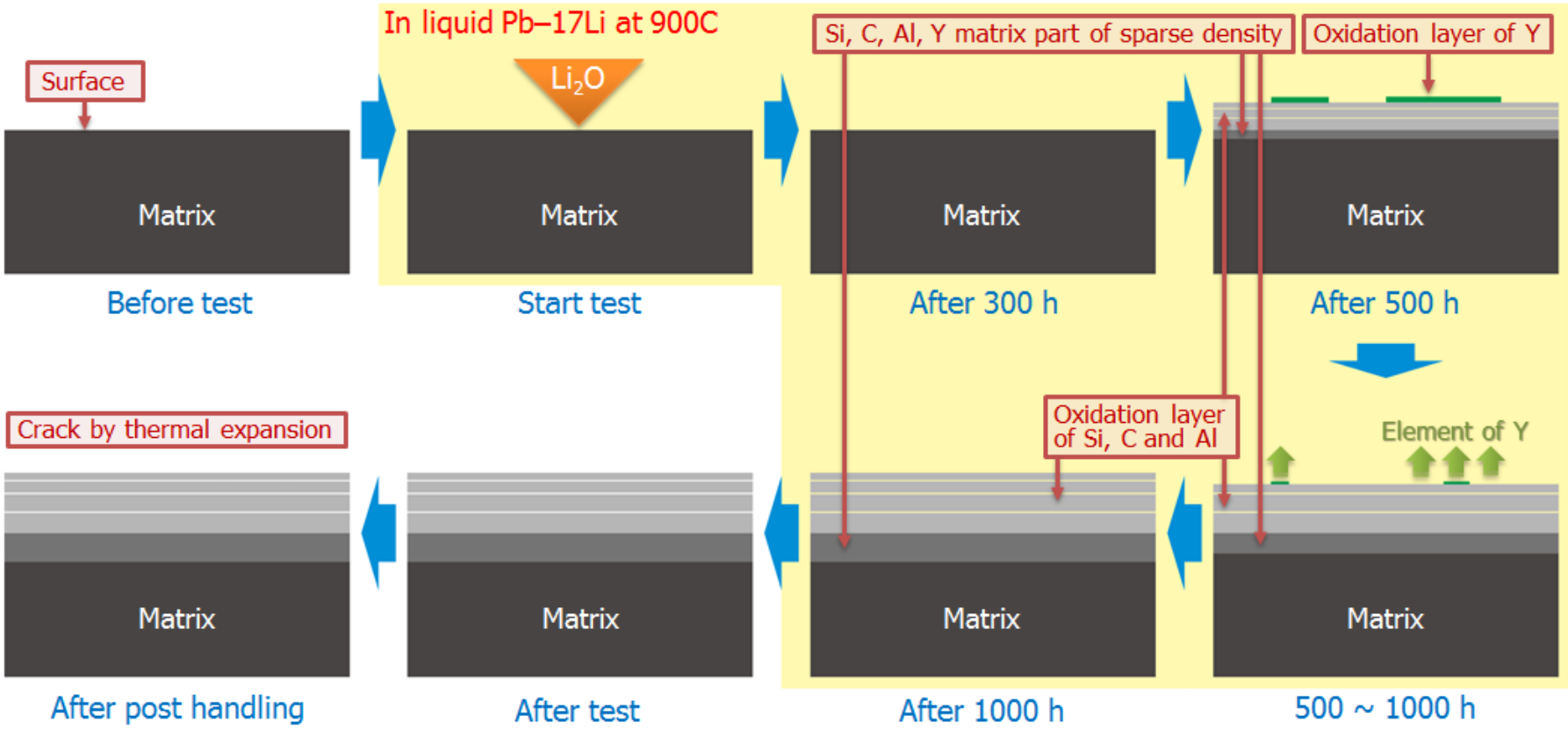


Figure 4.18 Schematic illustration of chemical reaction mechanism of NITE-SiC/SiC composite in flowing Pb–Li at 900℃.

## 4.4. Short summary of Chapter 4

Formation mechanism of the materials with and without sintering additive has been also examined by their activation energy and diffusion coefficient. After exposure at 900℃ with an < 0.01 ppm dissolved oxygen concentration for time periods up to 1000 h, transubstantial behavior of NITE–SiC/SiC composites and monolithic CVD–SiC materials has been investigated to make clear the effects of temperature and sintering additive by RD system. the transubstantial mechanism of SiC materials with and without sintering additive has been investigated. The results are summarized as follows:

1) It was difficult to detect Li by existing analysis equipment, however, detection of Li was possible by using of GD and SXES. As a result of analysis on the surface of specimen, the amount of the infiltration of Li, O and Pb was confirmed (Li > O > Pb).

2) In the case of monolithic CVD–SiC after exposure 900℃-1000 h, the layer that has not yet been reported to the static pot test for existing CVD–SIC was found, although there was no significant weight change. It was conformed that the transubstantial layer was formed at the edge of the specimen, which corresponded to contact velocity of 35–52 cm/s.

3) For the same condition of NITE–SiC/SiC composites, the transubstantial layer of specimen surface is produced by the Li–O (such as $Li_2O$) reaction between sintering additives and liquid Pb–Li. It was revealed that there is a relationship between contact speed and the thickness of the surface oxide layer. Furthermore, formation mechanism was discussed by evaluating the dependence of duration time.

# 5. Assessment of feasibility for the functional applications of SiC materials to blanket systems

## 5.1. Introduction

The liquid lithium–lead (Pb–Li) breeder blanket concept has been explored extensively in the European Union and the United States as a design option of DEMO blankets for fusion power reactors and test blanket modulus (TBMs) (HCLL—the helium cooled lithium–lead, DCLL—the dual cooled lithium–lead) testing in the International Thermonuclear Experimental Reactor (ITER) due to their potential attractiveness of economy, safety and relatively mature technology base [13, 48, 75-78].

The liquid Pb–Li blanket system is one of promising blanket concepts for fusion reactor [13, 75]. SiC and SiC/SiC composites are considered as one of the most promising high temperature structural material candidates for fusion blanket and as promising functional materials for flow channel insert (FCI) for Pb–Li blanket due to their excellent high temperature fracture, creep, corrosion and thermal shock resistance, and safety advantages arising from their low induced radioactivity and afterheat [48, 71]. In the TAURO, ARIES, DREAM and FDS-III blanket and power plant designs, SiC/SiC composites were considered as structural materials or FCIs and under wide research in the world [77-79]. Experiments on compatibility of SiC and SiC/SiC composites with liquid Pb–Li have been carried out in Japan, America, Europe and China. SiC/SiC composites are intrinsically porous material. Therefore an efficient densification or sealant is needed for blanket applications. The possibility to use SiC or SiC/SiC composite materials is under investigation.

In chapter 3 and 4, the formation behavior of the SiC materials in flowing Pb–Li was investigated in order to evaluate the system feasibility of the high temperature Pb–Li blanket for fusion reactor. The transubstantial layer on surface of monolithic CVD–SiC and NITE–SiC/SiC composites which contains Si, C, Al, Y and O was measured the electrical conductivity for electrical insulating ceramic materials. The electrical insulating ceramic materials on liquid metals are a promising technology for suppressing MHD pressure drop in the HT blanket systems. Advanced SiC materials are thought to be one of the potential candidate ceramic materials because of their high electrical resistivity and high compatibility with liquid metal Pb–Li. And compatibility problems are discussed for HT blanket system of fusion reactor design.

## 5.2. MHD pressure drop and flow channel inserts (FCIs)

Using flow channel inserts (FCIs) made of SiC/SiC composites for electrical insulation was proposed in [80]. In the present analysis, the US reference Dual Coolant Lithium Lead (DCLL) blanket is considered [81]. Reduced activation ferritic steel is used as the structural material. Helium cools the first wall and blanket structure, and the self-cooled breeder, Pb–Li, circulates for power conversion and tritium breeding. A key element of the concept is the SiC/SiC FCI (Figure 5.2) used as electric and thermal insulator. In the module the Pb–Li moves upward through the front channel, and then downward through two return channels. The Pb–Li flow both in the gap between the FCI and the wall and inside the FCI is driven by the same pressure head. There can be openings in one of the walls of the FCI to equalize the pressure on both sides of the FCI: either pressure equalization holes (PEH) or a pressure equalization slot (PES). The basic parameters are summarized in Table. We will refer to the flow inside the FCI as "bulk flow", and that in the gap as "gap flow". The channel sizes are identified with the internal FCI dimensions.

Due to safety and environmental reasons structural materials with the desired properties to produce the components facing the plasma in the fusion reactors must have a low neutron activation cross section, especially for the generation of long-lived isotopes. One of the materials incorporating this quality is the SiC and SiC/SiC composites which have high potential for fusion reactors since they can stand high working temperatures. The chemical compatibility with the breeder and neutron multiplier materials at temperatures above 900℃ is an important issue that must be addressed in order to make possible the use of SiC and SiC/SiC composites in fusion technology. In previous studies, we studied the chemical compatibility of SiC and SiC/SiC composites with liquid metal Pb–Li breeders at 900℃.

In the present study, we perform calculations in a parametric form. The electrical conductivity of SiC/SiC varied from 5 to 500 $(\Omega m)^{-1}$. Advice from material experts indicates that the lower values are in fact achievable. A thin sealing layer of crystal SiC was assumed at all surfaces of the FCI to prevent penetration of liquid metal [71].

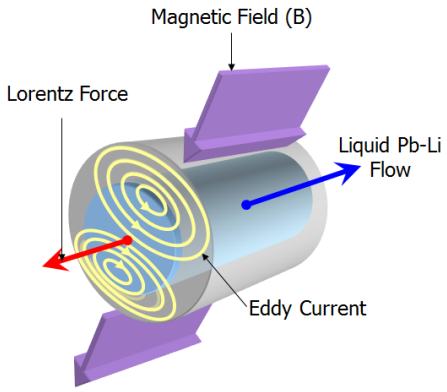


Figure 5.1 Phenomenon on MHD pressure drop.

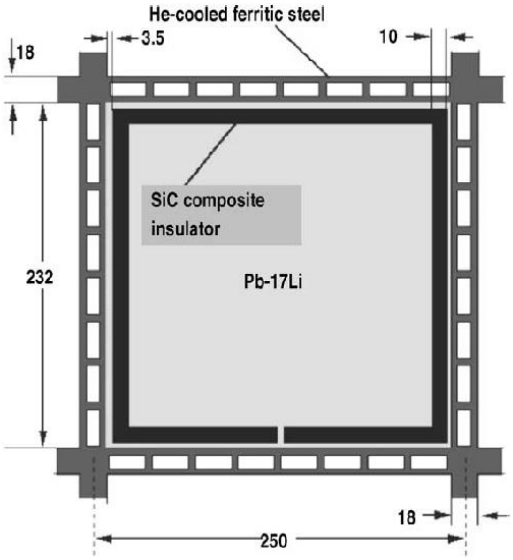


Figure 5.2 Typical poloidal blanket channel with FCI and helium cooling channels. Location of some of the helium channels is different for the front and return channels [82].

## 5.3. Compatibility problems for blanket system design

As seen here, sintering additives such as $SiO_2$, $Y_2O_3$ and $Al_2O_3$, for forming the material are affected in flowing liquid Pb–Li. However, it is to be able to say to all nuclear fusion materials, but it is so that more material is used in a region close to the limit of characteristics, as a matter of course, it has the relations that are close to a blanket system design.

In the nuclear fusion reactor concept that existed before, use of SiC materials is thought about in the blanket which pointed to a high efficiency and high temperature in particular, it use may

vary. At least, the SiC used in the blanket, there is also a side to be considered as a structural material, but a quite diverse function is also required, rather current structural material selection in the near future is limited to low-activation ferrite/martensitic steel, the role as the functional materials become important. Therefore, it may be misjudge the nature of the problem by applying the concept of corrosion, such as represented by the thinning and weakening of the normal structural material. Even material corrosion or denaturation of materials happens, it is able to withstand specifications unless significantly impaired large deformation or shape and strength of the molded body, on the other hand, a slight surface change may become fatal functionally.

This is same with aspect to aspect to radiation damage, environmental materials compatibility of SiC become a problem; all the lost or interaction with substances in contact, the degradation, the functions of various special features that are required as a blanket materials. In addition, on the other hand, it is not necessary to make a change a problem if they are not impaired. In particular, such as electrical conductivity and insulation capacity, thermal conductivity/thermal insulation, hydrogen permeability become the main target, yet the characteristic of interest them, because it must be evaluated by the change on the performance that is expected the reactor design, there is a design dependent on the compatibility problems. Or there is a constraint to the performance other than the direct target. For example, ceramic insulation was introduced in order to reduce the MHD pressure drop in liquid metal blanket, there is no problem DC electric conductivity must change, but the stability against resistive wall mode and one-turn resistance of plasma start-up response to the fluctuation electromagnetic field is affected.

Currently, it is not also present fusion reactor design using Pb–Li/SiC blanket that the details of the design up to this level. DCLL concept by the United States, DFLL concept by China, is the design of up to 900℃ level. And the system design with a tritium recovery system and heat exchanger has not yet been carried out. The authors assume the thermal utilization of 900℃ level using a Pb–Li/SiC blanket, and tested as described above in order to try to configure the heat exchanger be used SiC composites. Compatibility problems are always to influence the feasibility for the design concept, the maturation of the design is also what is needed in order to judge it.

## 5.4. Compatibility problems by formation of the transubstantial layer

The wall loss rate on the transubstantial layer of NITE–SiC/SiC composite with flowing condition of 20–25 cm/s is about 35 μm/yr. This value is not a problem for FCI to be used as

functional materials during operation period (2 years, continuous operation at 900℃). It is demanded from a design as an electrical insulation performance that keeps the conduction degree to lower than range of 100–300 S/m. In particular, from the fact that the transubstantial layer on surface of NITE–SiC/SiC composite is included Li oxidation compounds, such as $SiO_2$, $Li_4SiO_4$, $Li_2SiO_3$ and $LiAlO_3$ (lower electric conductivity than that of monolithic CVD–SiC, Figure 5.3), it is regarded that the impact of the formation of the transubstantial layer is small for operating at 900℃. It is expected that electrical conductivity changes of specimen with flowing condition in the liquid Pb–Li by the formation of the low-density transubstantial layer. However, as for the possible impacts, electrical conductivity of the NITE–SiC/SiC composite could be increased by the formation of the low-density transubstantial layer with micro-cracking that is infiltrated by flowing liquid Pb–Li. As a countermeasure, design by coating of CVD–SiC on the surface of the NITE–SiC/SiC is required to reduce the formation of the transubstantial layer.

And Figure 5.4 shows the time evolution of contact dose rate of fusion candidate materials. The radiation levels of ceramic materials used as FCI material down orders of magnitude $10^7$~$10^8$ within several weeks after a shot-down of fusion reactor. Although especially the required time of NITE–SiC/SiC composites by the influence of sintering additives is higher than that of monolithic CVD–SiC, the time of contact dose rate of NITE–SiC/SiC composites is shorter than that of RAFM F82H steel for blanket structural materials, the influence of sintering additives of NITE–SiC/SiC composites to irradiation damage does not become a problem about irradiation damage in design for fusion reactors.

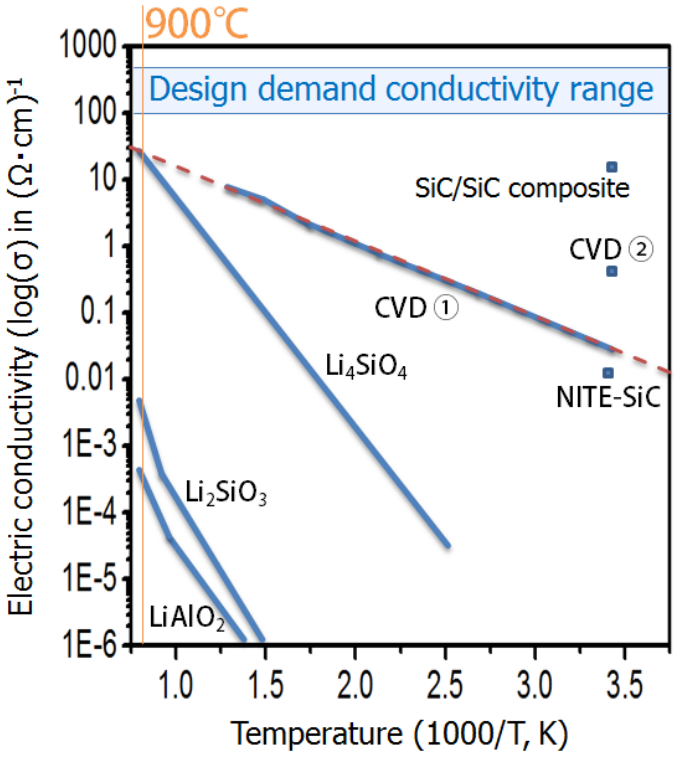


Figure 5.3 Electrical conductivity change by formation of the transubstantial layer.

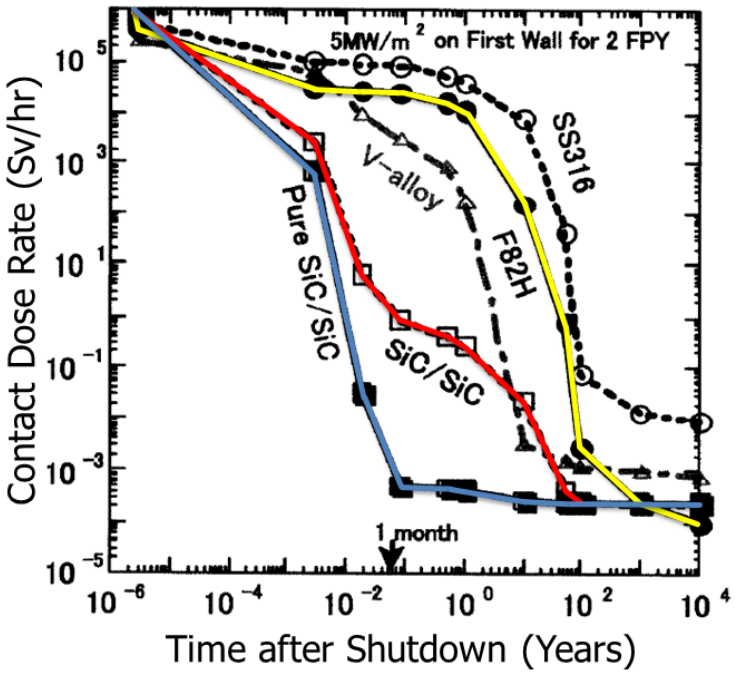


Figure 5.4 Time evolution of contact dose rate of fusion candidate materials [83].

## 5.5. Short summary of Chapter 5

In this chapter, the formation behavior of the transubstantial layer on the NITESiC materials surface in flowing Pb–Li was investigated and analyzed in order to evaluate the system feasibility of the high temperature Pb–Li blanket for fusion reactor. The transubstantial layer on surface of monolithic CVD–SiC and NITE–SiC/SiC composites which contains sintering additives was investigated the electrical conductivity for electrical insulating ceramic materials, in order to evaluate the system feasibility of the high temperature Pb–Li blanket for fusion reactor. And the compatibility problems for HT Pb–Li blanket system design were discussed. In particular, it is characteristic to note the design of the impact of the transubstantial layer be used to reduce the MHD pressure loss by the electrical insulation. Change in the electrical conductivity by Li composite oxidation has the potential to affect the electromagnetic characteristics and MHD pressure loss.

1) The change value of electric conductivity due to the formation rate and the shape of the transubstantial layer at 900℃ up to 1000 h, it is considered to form the oxidation with low-electrical conductivity, is rather less than SiC material before the transubstantial phenomenon. MHD pressure loss does not become a problem.

2) On the order hand, the formation of electric conduction layer due to the liquid metal PbLi infiltrates into the micro-cracking of the low-density transubstantial layer is a major problem. It is possible to coat the monolithic CVD–SiC material with low content of $SiO_2$ is effective in order to prevent this problem.

# 6. Conclusions and future works

## 6.1. Conclusions

Advanced SiC materials are expected to be promising as structural and/or functional materials for high temperature blanket systems, because of their good performance in high temperature strength, corrosion resistance and irradiation degradation. Until now, many efforts are underway to understand the relationship among microstructural characteristics (e.g. sintering additives and oxide reactants in Pb–Li) and formation mechanism on SiC materials exposed high temperature Pb–Li with flowing condition. Since the main purpose of this study was to give an overview design and details in the most important sections, studies based on scientific and engineering database were investigated. In general, innovations come up from these interests, thus these topics are introduced here as future works.

In this research, the compatibility evaluation technology of monolithic CVD–SiC and NITE–SiC/SiC composites with flowing liquid metal, which developed as structural and/or functional materials for next-generation fission and fusion blanket system, was introduced and improved. By using rotating disk system with flowing condition, the main objective is to investigate the formation mechanism of reaction layer between SiC material and liquid metal Pb–Li in the 900℃ which is suggested temperature for fuel manufacturing as hydrogen and fuel. From the obtained results, characteristic evaluation with flowing liquid metal Pb–Li at high temperature and feasibility was investigated for design of HT blanket system.

The following conclusions can be obtained from this work.

1) Development and improvement of technology compatibility evaluation technology for materials with flowing liquid metal:
   The rotating disk system which can quantitatively measure the various relative parameter (contact velocity, temperature, etc.) and confirm the relationship about compatibility is introduced and improved. By using this system, the method which can reveal the reaction on the specimen surface exposed to flowing liquid metal at high temperature was established in order to measure corrosion ratio with parameter of contact velocity at isothermal.

2) Investigation of formation mechanism on advanced SiC materials exposed liquid metal Pb–Li flowing:

Formation mechanism of reaction layer between SiC material and flowing liquid metal Pb–Li at 900C was revealed by Li–O reactant in liquid metal Pb–Li (both monolithic CVD–SiC and NITE–SiC/SiC composite) and sintering additives (such as $Y_2O_3$, $Al_2O_3$) in case of NITE–SiC/SiC composite.

3) Assessment of feasibility for the functional applications of SiC materials to blanket systems:

Attending to the restrictions characteristic (electrical conductivity and insulated capability) of advanced SiC materials at operation in the liquid metal Pb–Li at high temperature with flowing condition, evaluation on the compatibility problems expected on a blanket design was performed.

Since this study revealed that the biomass-fusion hybrid concept can be high temperature technology, compatibility research and electric conductivity, should be actively taken. In addition to the attractiveness of this concept, author believes that this study is a very first example of fusion reactor design study with considerations on the efficient application of fusion energy. It is the greatest pleasure for author if this study encourage following researcher to work with this concept and to consider other possible applications of fusion energy.

## 6.2. Future works

The RD system technology for compatibility evaluation with flowing condition at high temperature have been successfully developed, In addition, some areas of study that can benefit from further investigation for this work. Some of the potential researches are presented below.

1) Flow analysis of the rotating disk system with flowing condition

2) Compatibility tests of advanced SiC ceramic materials in liquid Pb–Li with magnetic field.

# References


[1] International energy outlook 2011 by IEA, (2011).

[2] World Energy Outlook 2012 by IEA.

[3] Shot-Term Energy Outlook 2013 by EIA.

[4] Annual Energy Outlook 2013 by EIA.

[5] BP Statistical Review of World Energy 2013, in, online at bp.com/statisticalreview, 2013.

[6] P. Norajitra, L. Buhler, U. Fischer, S. Gordeev, S. Malang, G. Reimann, Conceptual design of the dual-coolant blanket in the frame of the EU power plant conceptual study, Fusion Engineering and Design, 69 (2003) 669–673.

[7] N. Baluc, K. Abe, J.L. Boutard, V.M. Chernov, E. Diegele, S. Jitsukawa, A. Kimura, R.L. Klueh, A. Kohyama, R.J. Kurtz, R. Lasser, H. Matsui, A. Moslang, T. Muroga, G.R. Odette, M.Q. Tran, B. Van der Schaaf, Y. Wu, I. Yu, S.J. Zinkle, Status of R&D activities on materials for fusion power reactors, Nucl Fusion, 47 (2007) S696–S717.

[8] T. Muroga, T. Tanaka, A. Sagara, Blanket neutronics of Li/vanadium-alloy and Flibe/vanadium-alloy systems for FFHR, Fusion Engineering and Design, 81 (2006) 1203–1209.

[9] L.V. Boccaccini, L. Giancarli, G. Janeschitz, S. Hermsmeyer, Y. Poitevin, A. Cardella, E. Diegele, Materials and design of the European DEMO blankets, Journal of Nuclear Materials, 329 (2004) 148–155.

[10] M. Enoeda, M. Akiba, S. Tanaka, A. Shimizu, A. Hasegawa, S. Konishi, A. Kimura, A. Kohyama, A. Sagara, T. Muroga, Overview of design and R&D of test blankets in Japan, Fusion Engineering and Design, 81 (2006) 415–424.

[11] F. Najmabadi, A. Team, Overview of ARIES-RS tokamak fusion power plant, Fusion Engineering and Design, 41 (1998) 365–370.

[12] K. Ehrlich, E.E. Bloom, T. Kondo, International strategy for fusion materials development, Journal of Nuclear Materials, 283 (2000) 79–88.

[13] Y. Poitevin, L.V. Boccaccini, A. Cardella, L. Giancarli, R. Meyder, E. Diegele, R. Laesser, G. Benamati, The European breeding blankets development and the test strategy in ITER, Fusion Engineering and Design, 75–79 (2005) 741–749.

[14] T. Ihli, T.K. Basu, L.M. Giancarli, S. Konishi, S. Malang, F. Najmabadi, S. Nishio, A.R. Raffray, C.V.S. Rao, A. Sagara, Y. Wu, Review of blanket designs for advanced fusion reactors, Fusion Engineering and Design, 83 (2008) 912–919.

[15] K. Tobita, S. Nishio, M. Enoeda, H. Kawashima, G. Kurita, H. Tanigawa, H. Nakamura, M. Honda, A. Saito, S. Sato, T. Hayashi, N. Asakura, S. Sakurai, T. Nishitani, T. Ozeki, M. Ando, K. Ezato, K. Hamamatsu, T. Hirose, T. Hoshino, S. Ide, T. Inoue, T. Isono, C. Liu, S. Kakudate, Y. Kawamura, S. Mori, M. Nakamichi, H. Nishi, T. Nozawa, K. Ochiai, H. Ogiwara, N. Oyama, K. Sakamoto, Y. Sakamoto, Y. Seki, Y. Shibama, K. Shimizu, S. Suzuki, K. Takahashi, H. Tanigawa, D. Tsuru, T. Yamanishi, T. Yoshida, Compact DEMO, SlimCS: design progress and issues, Nucl Fusion, 49 (2009) 1–10.

[16] A. Sagara, H. Yamanishi, S. Imagawa, T. Muroga, T. Uda, T. Noda, S. Takahashi, K. Fukumoto, T. Yamamoto, H. Matsui, A. Kohyama, H. Hasizume, S. Toda, A. Shimizu, A. Suzuki, Y. Hosoya, S. Tanaka, T. Terai, D.K. Sze, O. Motojima, Design and development of the Flibe blanket for helical-type fusion reactor FFHR, Fusion Engineering and Design, 49–50 (2000) 661–666.

[17] C.P.C. Wong, M. Abdou, M. Dagher, Y. Katoh, R.J. Kurtz, S. Malang, E.P. Marriott, B.J. Merrill, K. Messadek, N.B. Morley, M.E. Sawan, S. Sharafat, S. Smolentsev, D.K. Sze, S. Willms, A. Ying, M.Z. Youssef, An overview of the US DCLL ITER-TBM program, Fusion Engineering and Design, 85 (2010) 1129–1132.

[18] K. Tobita, S. Nishio, M. Sato, S. Sakurai, T. Hayashi, Y.K. Shibama, T. Isono, M. Enoeda, H. Nakamura, S. Sato, K. Ezato, T. Hayashi, T. Hirose, S. Ide, T. Inoue, Y. Kamada, Y. Kawamura, H. Kawashima, N. Koizumi, G. Kurita, Y. Nakamura, K. Mouri, T. Nishitani, J. Ohmori, N. Oyama, K. Sakamoto, S. Suzuki, T. Suzuki, H. Tanigawa, K. Tsuchiya, D. Tsuru, SlimCS-compact low aspect ratio DEMO reactor with reduced-size central solenoid, Nucl Fusion, 47 (2007) 892–899.

[19] H. Chen, Y. Wu, S. Konishi, J. Hayward, A high temperature blanket concept for hydrogen production, Fusion Engineering and Design, 83 (2008) 903–911.

[20] R. Moreau, P. Leroy, An estimation of MHD effects in the European water-cooled lithium–lead blanket, Fusion Engineering and Design, 17 (1991) 227–231.

[21] K.A. Mccarthy, M.A. Abdou, Analysis of liquid metal MHD flow in multiple adjacent ducts using an iterative method to solve the core flow equations, Fusion Engineering and Design, 13 (1991) 363–380.

[22] Y. Katoh, A. Kohyama, T. Nozawa, M. Sato, SiC/SiC composites through transient eutectic-phase route for fusion applications, Journal of Nuclear Materials, 329 (2004) 587-591.

[23] S.M. Dong, Y. Katoh, A. Kohyama, Preparation of SiC/SiC composites by hot pressing, using Tyranno-SA fiber as reinforcement, J Am Ceram Soc, 86 (2003) 26–32.

[24] M. Kondo, T. Muroga, T. Nagasaka, Q. Xu, V. Tsisar, T. Oshima, Mass transfer of RAFM steel in Li by simple immersion, impeller induced flow and thermal convection, Journal of Nuclear Materials, 417 (2011) 1200–1204.

[25] M. Kondo, M. Takahashi, T. Tanaka, V. Tsisar, T. Muroga, Compatibility of reduced activation ferritic martensitic steel JLF-1 with liquid metals Li and Pb–17Li, Fusion Engineering and Design, 87 (2012) 1777–1787.

[26] V. Coen, P. Fenici, Compatibility of structural materials with liquid breeders – a review of recent work carried out at JRC, ISPRA, Nuclear Engineering and Design/Fusion, 1 (1984) 215–229.

[27] O.K. Chopra, P.F. Tortorelli, Compatibility of materials for use in liquid–metal blankets of fusion reactors, Journal of Nuclear Materials, 122&123 (1984) 1201–1212.

[28] O.K. Chopra, D.L. Smith, Compatibility of ferritic steels in forced circulation lithium and Pb–17Li systems, Journal of Nuclear Materials, 155 (1988) 715–721.

[29] O.K. Chopra, D.L. Smith, Corrosion Behavior of Vanadium Alloys in Flowing Lithium, Journal of Nuclear Materials, 155 (1988) 683–689.

[30] H. Tas, J. Dekeyser, F. Casteels, J. Walnier, F. Deschutter, Mass transfer in pure lithium and lithium–lead dynamic environments: Influence of system parameters, Journal of Nuclear Materials, 141 (1986) 571–578.

[31] M. Broc, T. Flament, P. Fauvet, J. Sannier, Corrosion of Austenitic and Martensitic Stainless-Steels in Flowing 17Li–83Pb Alloy, Journal of Nuclear Materials, 155 (1988) 710–714.

[32] P. Hubberstey, Pb–17Li and lithium: A thermodynamic rationalisation of their radically different chemistry, Journal of Nuclear Materials, 247 (1997) 208–214.

[33] A. Terlain, T. Dufrenoy, Influence of a magnetic field on the corrosion of austenitic and martensitic steels by semi-stagnant Pb17Li, Journal of Nuclear Materials, 212 (1994) 1504–1508.

[34] F. Barbier, A. Alemany, S. Martemianov, On the influence of a high magnetic field on the corrosion and deposition processes in the liquid Pb–17Li alloy, Fusion Engineering and Design, 43 (1998) 199–208.

[35] B.A. Pint, J.L. Moser, P.F. Tortorelli, Investigation of Pb–Li compatibility issues for the dual coolant blanket concept, Journal of Nuclear Materials, 367 (2007) 1150–1154.

[36] H. Glasbrenner, J. Konys, H.D. Röhrig, K. Stein-Fechner, Z. Voss, Corrosion of ferritic–martensitic steels in the eutectic Pb–17Li, Journal of Nuclear Materials, 283 (2000) 1332–1335.

[37] J. Konys, W. Krauss, J. Novotny, H. Steiner, Z. Voss, O. Wedemeyer, Compatibility behavior of EUROFER steel in flowing Pb–17Li, Journal of Nuclear Materials, 386–88 (2009) 678–681.

[38] Q.Y. Huang, S. Gao, Z.Q. Zhu, M.L. Zhang, Y. Song, C.J. Li, Y.P. Chen, X.Z. Ling, X.G. Zhou, Progress in compatibility experiments on lithium–lead with candidate structural materials for fusion in China, Fusion Engineering and Design, 84 (2009) 242–246.

[39] H.U. Borgstedt, H. Feuerstein, The solubility of metals in Pb–17Li liquid alloy, Journal of Nuclear Materials, 191 (1992) 988–991.

[40] J. Konys, W. Krauss, Z. Voss, O. Wedemeyer, Corrosion behavior of EUROFER steel in flowing eutectic Pb–17Li alloy, Journal of Nuclear Materials, 329 (2004) 1379–1383.

[41] J. Konys, W. Krauss, Z. Voss, O. Wedemeyer, Comparison of corrosion behavior of bare and hot-dip coated EUROFER steel in flowing Pb–17Li, Journal of Nuclear Materials, 367 (2007) 1144–1149.

[42] G. Benamati, C. Fazio, I. Ricapito, Mechanical and corrosion behaviour of EUROFER 97 steel exposed to Pb–17Li, Journal of Nuclear Materials, 307–311 (2002) 1391–1395.

[43] M.G. Barker, V. Coen, H. Kolbe, J.A. Lees, L. Orecchia, T. Sample, The effect of oxygen impurities on the behavior of type 316 stainless steel in Pb–17Li, Journal of Nuclear Materials, 155 (1988) 732–735.

[44] N. Simon, A. Terlain, T. Flament, The compatibility of martensitic steels with liquid Pb–17Li, Journal of Nuclear Materials, 254 (1998) 185–190.

[45] N. Simon, A. Terlain, T. Flament, The compatibility of austenitic materials with liquid Pb–17Li, Corros Sci, 43 (2001) 1041–1052.

[46] P.F. Tortorelli, J.H. Devan, Corrosion of ferrous alloys exposed to thermally convective Pb–17 at% Li, Journal of Nuclear Materials, 141 (1986) 592–598.

[47] O.K. Chopra, D.L. Smith, Compatibility of ferrous alloys in a forced circulation Pb–17Li system, Journal of Nuclear Materials, 141 (1986) 566–570.

[48] H.U. Borgstedt, M. Grundmann, The influence of liquid Pb–17Li eutectic on the mechanical properties of structural materials, Fusion Engineering and Design, 6 (1988) 155–158.

[49] J. Sannier, M. Broc, T. Flament, A. Terlain, Corrosion of austenitic and martensitic stainless steels in flowing Pb17Li alloy, Fusion Engineering and Design, 14 (1991) 299–307.

[50] I. Bucenieks, R. Krishbergs, E. Platacis, G. Lipsbergs, A. Shishko, A. Zik, F. Muktepavela, Investigation of corrosion phenomena in eurofer steel in Pb–17Li stationary flow exposed to a magnetic field, Magnetohydrodynamics, 42 (2006) 237–251.

[51] M. Kondo, T. Muroga, A. Sagara, T. Valentyn, A. Suzuki, T. Terai, M. Takahashi, N. Fujii, Y. Yokoyama, H. Miyamoto, E. Nakamura, Flow accelerated corrosion and erosion–corrosion of RAFM steel in liquid breeders, Fusion Engineering and Design, 86 (2011) 2500–2503.

[52] G.A. L. Giancarli, A. Caso, A. Gasse, G. Le Marois, Y. Poitevin, J.F. Salavy, J. Szczepanski, R&D issues for $SiC_f$/SiC composites structural material in fusion power reactor blankets, Fusion Engineering and Design, 48 (2000) 509–520.

[53] B. Riccardi, A.F.R. P. Fenici, L. Giancarli, G. Le Marois, E. Philippe, Status of the European R&D activities on $SiC_f$/SiC composites for fusion reactors, Fusion Engineering and Design, 51–52 (2000) 11–22.

[54] B.A. Pint, L.D. Chitwood, J.R. Di Stefano, Long-term stability of ceramics in liquid lithium, Journal of Nuclear Materials, 289 (2001) 52–56.

[55] A.R. Raffray, R. Jones, G. Aiello, M. Billone, L. Giancarli, H. Golfier, A. Hasegawa, Y. Katoh, A. Kohyama, S. Nishio, B. Riccardi, M.S. Tillack, Design and material issues for high performance $SiC_f$/SiC-based fusion power cores, Fusion Engineering and Design, 55 (2001) 55–95.

[56] Y. Wu, Design status and development strategy of China liquid lithium–lead blankets and related material technology, Journal of Nuclear Materials, 367 (2007) 1410–1415.

[57] Z.Q. Zhu, Q.Y. Huang, S. Gao, X.G. Zhou, X.Z. Ling, Y.P. Chen, M.L. Zhang, Y. Song, Y.L. Wang, Z.F. Zhang, S. Zhao, M.G. Kong, Preliminary experiment on compatibility of $SiC_f$/SiC composites in static liquid LiPb at 700 degrees C, Fusion Engineering and Design, 84 (2009) 2048–2051.

[58] A. Hasegawa, A. Kohyama, R.H. Jones, L.L. Snead, B. Riccardi, P. Fenici, Critical issues and current status of SiC/SiC composites for fusion, Journal of Nuclear Materials, 283 (2000) 128–137.

[59] R.H. Jones, L. Giancarli, A. Hasegawa, Y. Katoh, A. Kohyama, B. Riccardi, L.L. Snead, W.J. Weber, Promise and challenges of $SiC_f$/SiC composites for fusion energy applications, Journal of Nuclear Materials, 307 (2002) 1057-1072.

[60] B. Riccardi, L. Giancarli, A. Hasegawa, Y. Katoh, A. Kohyama, R.H. Jones, L.L. Snead, Issues and advances in $SiC_f$/SiC composites development for fusion reactors, Journal of Nuclear Materials, 329 (2004) 56–65.

[61] F. Barbier, P. Deloffre, A. Terlain, Compatibility of materials for fusion reactors with Pb–17Li, Journal of Nuclear Materials, 307 (2002) 1351–1354.

[62] B.A. Pint, J.L. Moser, R. Tortorelli, Liquid metal compatibility issues for test blanket modules, Fusion Engineering and Design, 81 (2006) 901–908.

[63] H. Kleykamp, Compatibility studies in the Li17Pb83–SiC, Be–SiC and Be–Mo systems, Journal of Nuclear Materials, 321 (2003) 170–176.

[64] P.F. Tortorelli, Corrosion of Ferritic Steels by Molten Lithium - Influence of Competing Thermal-Gradient Mass-Transfer and Surface Product Reactions, Journal of Nuclear Materials, 155 (1988) 722–727.

[65] M. Kondo, T. Nagasaka, V. Tsisar, A. Sagara, T. Muroga, T. Watanabe, T. Oshima, Y. Yokoyama, H. Miyamoto, E. Nakamura, N. Fujii, Corrosion of reduced activation ferritic martensitic steel JLF-1 in purified Flinak at static and flowing conditions, Fusion Engineering and Design, 85 (2010) 1430–1436.

[66] M. Kondo, M. Takahashi, T. Suzuki, K. Ishikawa, K. Hata, S.Z. Qiu, H. Sekimoto, Metallurgical study on erosion and corrosion behaviors of steels exposed to liquid lead–bismuth flow, Journal of Nuclear Materials, 343 (2005) 349–359.

[67] C. Park, K. Noborio, R. Kasada, Y. Yamamoto, G. Nam, S. Konishi, Compatibility of materials for advanced blanket with liquid LiPb, 2009 23rd Ieee/Npss Symposium on Fusion Engineering, (2009) 293–296.

[68] C. Park, K. Noborio, R. Kasada, Y. Yamamoto, S. Konishi, Compatibility of $SiC_f$/SiC composite exposed to liquid Pb–Li flow, Journal of Nuclear Materials, 417 (2011) 1218–1220.

[69] B.A. Pint, J.L. Moser, A. Jankowski, J. Hayes, Compatibility of multi-layer, electrically insulating coatings for vanadium–lithium blankets, Journal of Nuclear Materials, 367 (2007) 1165–1169.

[70] 谷川博康, 関洋治, 廣瀬貴規, 江里幸一郎, 谷川尚, 鶴大悟, 吉河朗, 榎枝幹男, 大図章, 呉田昌俊, Private community, (2013).

[71] S. Smolentsev, M. Abdou, N.B. Morley, M. Sawan, S. Malang, C. Wong, Numerical analysis of MHD flow and heat transfer in a poloidal channel of the DCLL blanket with a $SiC_f$/SiC flow channel insert, Fusion Engineering and Design, 81 (2006) 549–553.

[72] Y. Yamamoto, T. Yamanishi, Y. Kawamura, K. Isobe, Y. Yamamoto, S. Konishi, Fundamental study on purity control of the liquid metal blanket using solid electrolyte cell, Fusion Sci Technol, 52 (2007) 692–695.

[73] C.-H. Doh, A. Veluchamy, M.-W. Oh, B.-C. Han, Analysis on the formation of $Li_4SiO_4$ and $Li_2SiO_3$ through first principle calculations and comparing with experimental data related to lithium battery, Journal of Electrochemical Science and Technology, 2 (2011) 146–151.

[74] P. Hubberstey, Pb-17Li and lithium: A thermodynamic rationalisation of their radically different chemistry, Journal of Nuclear Materials, 247 (1997) 208-214.

[75] D. Maisonnier, I. Cook, S. Pierre, B. Lorenzo, D.P. Luigi, G. Luciano, N. Prachai, P. Aldo, DEMO and fusion power plant conceptual studies in Europe, Fusion Engineering and Design, 81 (2006) 1123–1130.

[76] Y. Poitevin, M.A. Futterer, L. Giancarli, A.L. Puma, J.F. Salavy, J. Szczepanski, Status of the design and performances of the WCLL test blanket module for ITER-FEAT, Fusion Engineering and Design, 61–62 (2002) 431–437.

[77] D.K. Sze, M. Tillack, L. El-Guebaly, Blanket system selection for the ARIES-ST, Fusion Engineering and Design, 48 (2000) 371–378.

[78] P. Sardain, D. Maisonnier, L. Di Pace, L. Giancarli, A.L. Puma, P. Norajitra, A. Orden, E. Arenaza, D. Ward, The European power plant conceptual study: Helium-cooled lithium–lead reactor concept, Fusion Engineering and Design, 81 (2006) 2673–2678.

[79] Y. Wu, Conceptual design activities of FDS series fusion power plants in China, Fusion Engineering and Design, 81 (2006) 2713–2718.

[80] S. Malang, M.S. Tillack, High performance PbLi blanket, in: Proceedings of the17th IEE/NPSS Symposium on Fusion Engineering, 2 (1997) 1000–1004.

[81] C. Wong, S. Malang, M. Sawan, S. Smolentsev, S. Majumdar, B. Merrill, D. Sze, N. Morley, S. Sharafat, P. Fogarty, M. Dagher, P. Peterson, H. Zhao, S. Zinkle, M. Youssef, Assessment of liquid breeder first wall and blanket options for the DEMO design, in: Proceedings of the 16th ANS TOFE Meeting, Madison, September, 14–16 (2004).

[82] M.A. S. Smolentsev, N.B. Morley, M. Sawan, S. Malang, C. Wong, Numerical analysis of MHD flow, heat transfer and tritium transport in a poloidal channel of the DCLL blanket with a SiCf/SiC flow channel insert, Fusion Engineering and Design, 81 (2005) 549–553.

[83] M. Chen, Q. Huang, S.L. Zheng, Activation analysis of tritium breeder materials in the FDS-II fusion power reactor, Fusion Engineering and Design, 82 (2007) 2641–2646.

# List of publications


[1] C. Park, K. Noborio, R. Kasada, Y. Yamamoto, G. Nam, S. Konishi, Compatibility of materials for advanced blanket with liquid LiPb, In Fusion Engineering, 2009. SOFE 2009. 23rd IEEE/NPSS Symposium on IEEE (2009) 1–4.

[2] Y. Yamamoto, D. Kim, C. Park, S. Konishi, Development of high temperature particle load test equipment by hydrogen ion beam for divertor, In Fusion Engineering, 2009. SOFE 2009. 23rd IEEE/NPSS Symposium on IEEE (2009) 1–4.

[3] Y. Takeuchi, C. Park, K. Noborio, Y. Yamamoto, S. Konishi, Heat Transfer in SiC Compact Heat Exchanger, Fusion Engineering and Design, 85 (2010) 1266–1270.

[4] S. Konishi, C. Park, R. Kasada, K. Noborio, Compatibility of SiC in Liquid Blanket", Journal of Plasma and Fusion Research, 86 (2010) 417–419.

[5] C. Park, K. Noborio, R. Kasada, Y. Yamamoto, S. Konishi, Compatibility of $SiC_f$/SiC Composite Exposed to Liquid LiPb Flow, Journal of Nuclear Materials, 417 (2011) 1218–1220.

# List of presentations

[1] 朴昶虎, 登尾一幸, 山本靖, 小西哲之, 高温 LiPb と材料の共存性, 第 7 回連合講演会, 青森市民ホール, 日本, 2008. 6. 19.

[2] C. Park, K. Noborio, R. Kasada, Y. Yamamoto, S. Konishi, Compatibility of materials for advanced blanket with liquid LiPb, 18th Topical Meeting on the Technology of Fusion Energy, The Stanford Court Hotel, San Francisco, CA, USA, 2008. 9. 28.

[3] 朴昶虎, 登尾一幸, 笠田, 山本靖, 小西哲之, 高温液体 LiPb と材料の共存性, 第 25 回プラズマ・核融合学会年会, 栃木県総合文化センター, 日本, 2008. 12. 2.

[4] 山本靖, 金度亨, 朴昶虎, 小西哲之, 水素イオンビームによる高熱粒子負荷実験装置の開発, 第25回プラズマ・核融合学会年会, 栃木県総合文化センター, 日本, 2008. 12. 2.

[5] C. Park, K. Noborio, R. Kasada, Y. Yamamoto, S. Konishi, Compatibility of materials for advanced blanket with liquid LiPb, Korea-Japan International Workshop on Fusion Reactor materials, Pukyong University, Busan, Korea, 2009. 3. 19.

[6] C. Park, K. Noborio, R. Kasada, Y. Yamamoto, G. Nam, S. Konishi, Compatibility of materials for advanced blanket with liquid LiPb, 23rd Symposium on Fusion Engineering, Omni hotel, San Diego, CA, USA, 2009. 5. 31.

[7] Y. Yamamoto, D. Kim, C. Park, S. Konishi, Development of high temperature particle load test equipment by hydrogen ion beam for divertor, 23rd Symposium on Fusion Engineering, Omni hotel, San Diego, CA, USA, 2009. 5. 31.

[8] C. Park, K. Noborio, R. Kasada, Y. Yamamoto, S. Konishi, Compatibility of $SiC_f$/SiC composite exposed to liquid LiPb flow, 14th International Conference on Fusion Reactor Materials, Sapporo Convention Center, Sapporo, Japan, 2009. 9. 6.

[9] Y. Takeuchi, C. Park, K. Noborio, Y. Yamamoto, S. Konishi, Heat transfer in SiC compact heat exchanger, 9th International Symposium on Fusion Nuclear Technology, Furama Hotel, Dalian, China, 2009. 10. 11.

[10] 山本靖, 金度亨, 朴昶虎, 小西哲之, 水素イオンビームによる高熱粒子負荷実験装置の開発, 原型炉設計プラットフォーム会合, 青森, 日本, 2009. 10. 29.

[11] C. Park, K. Noborio, R. Kasada, Y. Yamamoto, S. Konishi, Compatibility of $SiC_f$/SiC composite exposed to liquid LiPb flow, Asian-Core Winter School Technical Program, APA Hotel & Resort Sapporo, Sapporo, Japan, 2010. 2. 22.

[12] C. Park, K. Noborio, R. Kasada, Y. Yamamoto, S. Konishi, Compatibility of NITE–SiC composites exposed to liquid Pb–Li flow, Asian-Core International Symposium on Advanced Energy Systems and Materials, Pukyong University, Busan, Korea, 2011. 3. 4.

[13] C. Park, K. Noborio, Y. Yamamoto, S. Konishi, Compatibility of SiC exposed to liquid Pb–Li flow for development of SiC-LiPb blanket and divertor component, International Symposium on Fusion Nuclear Technology 10, Portland, Oregon, USA, 2011. 9. 13.

[14] 朴昶虎, G. NAM, 笠田竜太, 小西哲之, 900℃の液体金属鉛リチウム中の$SiC_f$/SiC複合材の共存性, 第9回核融合エネルギー連合講演会, 日本, 2012. 6. 28.

[15] C. Park, G. Nam, R. Kasada, S. Konishi, Compatibility of $SiC_f$/SiC composite material exposed to liquid Pb–Li at 900℃, Asian-Core University Program on Advanced Energy Science, International Symposium on Advanced Energy Systems and Materials, Aomori, Japan, 2012. 8. 22.

[16] C. Park, R. Kasada, S. Konishi, Microstructural and corrosion behavior of $SiC_f$/SiC composite material exposed to liquid Pb–Li at 900℃, Nuclear Materials Conference 2012, Osaka, Japan, 2012. 10. 23.

[17] 朴昶虎, 笠田竜太, 小西哲之, 900℃の液体金属鉛リチウム中の$SiC_f$/SiC複合材の腐食挙動と構造, 第3回原型炉設計プラットフォーム会合, 青森, 日本, 2012. 11. 14.

# List of award

[1] C. Park, K. Noborio, R. Kasada, Y. Yamamoto, S. Konishi, Compatibility of NITE–SiC composites exposed to liquid Pb–Li flow, Asian-Core International Symposium on Advanced Energy Systems and Materials, Pukyong University, Busan, Korea, 2011. 3. 4.

# Acknowledgement

Kyoto's life in Japan was perfect time for me to learn things I haven't seen enough. There were many opportunities to see students and scientists not only in the fusion area but also in different scientific fields. Experiences with all of them were essential to complete this study.

I would like to first express my deep gratitude to my supervisor, Professor Dr. Satoshi Konishi, Kyoto University for his encouragement, suggestions, guidance and many discussions throughout this study. I was always surprised by his innovative ideas came up from his unique sight on things. Prof. Kasada always helped my study. I totally respect his toughness and attitude to research. I was always surprised by his innovative ideas came up from his unique sight on things. Working with him, my engineering knowledge and skills truly improved. Prof. Yamamoto from Kansai University gave advices about the electric experiment. I deep thank Prof. Takeuchi for his meaningful advice. Dr. Noborio always gave me technical helps. It was a joy to do experimental work with him. Working with very unique colleagues, 30 students in total and a clerical assistant, in Konishi Lab was really friendly. I learned many lessons through teaching them basic skills. Discussions with them always gave me a new sight for my research. I thank Ms. Junko Kobayashi and Hiroko Miyuki for their support on clerical works.

I didn't forget to say, this work was partially supported by the Global COE program of Kyoto University "toward $CO_2$ Zero-emission System."